JACS
JOURNAL OF THE AMERICAN CHEMICAL SOCIETY

ARTICLE

pubs.acs.org/JACS

Regioselective Lithium Diisopropylamide-Mediated Ortholithiation of 1-Chloro-3-(trifluoromethyl)benzene: Role of Autocatalysis, Lithium Chloride Catalysis, and Reversibility

Alexander C. Hoepker, Lekha Gupta, Yun Ma, Marc F. Faggin, and David B. Collum*

Department of Chemistry and Chemical Biology, Baker Laboratory, Cornell University, Ithaca, New York 14853-1301, United States

Supporting Information

ABSTRACT: Ortholithiation of 1-chloro-3-(trifluoromethyl) benzene with lithium diisopropylamide (LDA) in tetrahydrofuran at −78 °C displays characteristics of reactions in which aggregation events are rate limiting. Metalation with lithium-chloride-free LDA involves a rate-limiting deaggregation via dimer-based transition structures. The post-rate-limiting proton transfers are suggested to involve highly solvated triple ions. Autocatalysis by the resulting aryllithiums or catalysis by traces (<100 ppm) of LiCl diverts the reaction through di- and trisolvated monomer-based pathways for metalation at the 2 and 6 positions, respectively. The regiochemistry is dictated by a combination of kinetically controlled metalations overlaid by an equilibration involving diisopropylamine that is shown to occur by the microscopic reverse of the monomer-based metalations.

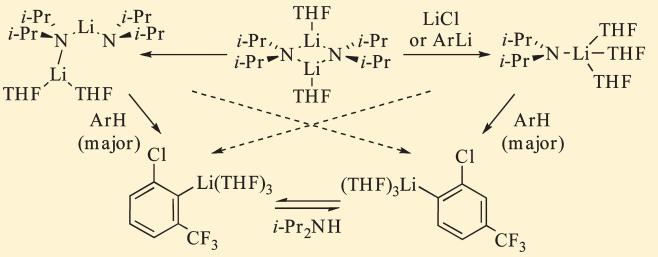

INTRODUCTION

Equation 1 illustrates lithium-amide-mediated ortholithiations of **1** first studied by Schlosser and co-workers.[1] Divergent regioselectivities derived from lithium diisopropylamide (LDA) and lithium 2,2,6,6-tetramethylpiperidide (LiTMP) have been observed for ortholithiations and are often attributed to steric effects.[2] Further experiments, however, show this to be too simplistic. The reactions are extraordinarily sensitive to the source of LDA: *commercially purchased LDA prepared from styrene and lithium metal is approximately 10 times less reactive than LDA generated using n-BuLi and i-Pr$_2$NH, and the regioselectivities are similar but not identical.* Monitoring reactions of analytically pure LDA[3] using in situ IR and ^{19}F NMR spectroscopies uncovers additional oddities. Addition of low concentrations of arene **1** affords a linear disappearance of **1** and a slight drift in regioselectivity that continues after the metalation is complete (Figure 1A). Ortholithiation using higher substrate concentrations (Figure 1B) affords a sigmoidal disappearance of arene **1** and a distribution of regioisomers **2** and **3** that changes markedly over time. Traces of LiCl added to a reaction in progress causes a burst of reactivity that displays upward curvature (Figure 2).

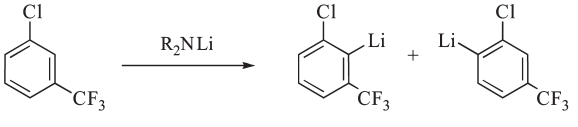

(1)

1 **2** **3**

LDA/ THF/ -78 °C 1:1.5
LDA/ THF/ -60 °C >40:1
LiTMP/ THF/ -78 °C 1:20

We describe herein rate and mechanistic studies of the ortholithiation in eq 1 that support the simplified mechanistic scenario summarized in Scheme 1, studies which culminated in the best-fit numerical integrations displayed in Figure 1. The high regioselectivity of the reaction at −60 °C derives from an equilibration of aryllithiums (**2a** and **3a**), which is discussed in detail.[4,5] The really interesting part of this story, however, is what lurks beneath the 2:1 selectivity using LDA in tetrahydrofuran (THF) at −78 °C. The ortholithiation of **1** joins a growing class of LDA-mediated transformations in which the fragmentation of LDA dimer **4** is rate limiting.[3,6,7] Reactions within this class proceed at −78 °C, conditions prevalent in organic chemistry,[8] and are prone to both autocatalysis as well as catalysis by traces of LiCl and other exogenous lithium salts.[8,9] The ortholithiation of **1** introduces two prominent dimensions absent in previous studies: (1) aryllithiums **2a** and **3a** are inequivalent autocatalysts, and (2) the uncatalyzed and catalyzed lithiations proceed via distinctly different fleeting structural forms of LDA (**5** and **6**).

The results section offers a view of *how* the mechanisms were determined. The data are highly interdependent but are necessarily presented linearly. Evidence supporting the conclusions paints a compelling picture when considered collectively. The discussion begins with a summary, which is followed by analyses of rate-limiting deaggregation, LiCl catalysis, autocatalysis, and aryllithium (ArLi) equilibration. The conclusion considers the implications from the divergent perspectives of mechanistic and synthetic organic chemists.

Received: January 29, 2011
Published: April 18, 2011

dx.doi.org/10.1021/ja200906z | J. Am. Chem. Soc. 2011, 133, 7135–7151

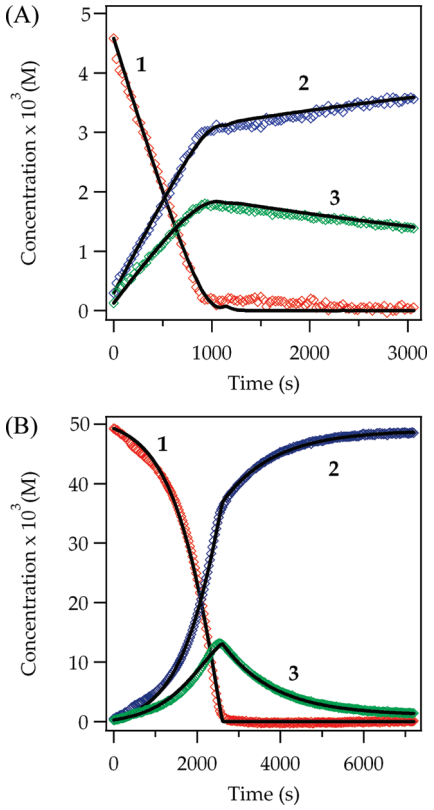

Figure 1. Representative plots of concentration versus time monitored by ^{19}F NMR spectroscopy for the ortholithiation of **1** and formation of **2** and **3** by LDA (0.10 M) in THF (12.2 M) at −60 °C: (A) 0.005 M **1**; (B) 0.050 M **1**. The curves represent best-fit numerical integrations as described below.

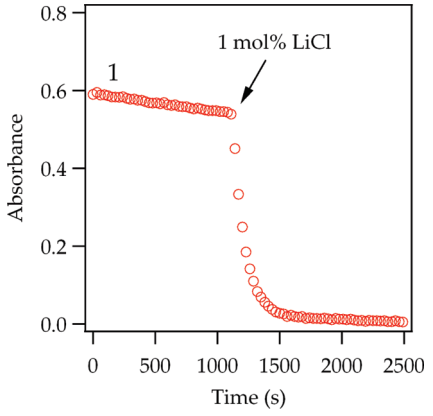

Figure 2. Ortholithiation of **1** (0.010 M) with LDA (0.10 M) in THF (12.2 M) at −78 °C monitored by IR spectroscopy (1325 cm^{-1}) with injection of 1.0 mol % LiCl (0.001 M).

RESULTS

Solution Structures. Structural assignments of LDA and aryllithiums are required to interpret the rate data. Previous studies of [^{6}Li,^{15}N]LDA using ^{6}Li and ^{15}N NMR spectroscopies[10] reveal exclusively disolvated dimer **4**.[11] The ^{13}C NMR spectra of aryllithiums **2** and **3** display 1:1:1 triplets for the lithiated carbons.[12] The triplet corresponding to **2** is further split by ^{19}F−^{13}C coupling, whereas no such coupling is observed for **3**. The ^{19}F{^{1}H}NMR spectra display singlets.[13] Generating **2** and **3** with excess [^{6}Li,^{15}N]LDA shows no ^{6}Li−^{15}N splitting in the ^{6}Li resonances of **2** and **3**, confirming the absence of mixed aggregation.[10] Comparing **1** recovered from quenching metalations using D_2O with authentic samples prepared from the corresponding aryl bromides[14] confirm the assignments. Density functional theory (DFT) computations at the B3LYP/6-31G(d) level[15] with single-point calculations at the MP2 level of theory implicate trisolvated monomers (**2a** and **3a**; Scheme 1) in accord with other monomeric aryllithiums.[16] References to **2a** and **3a** are used instead of **2** and **3** when the structural details need to be specified. Under conditions of LiCl catalysis (<5.0 mol % LiCl), LiCl has been shown to exist exclusively as an 8:1 mixture of mixed trimer **7** and dimer **8**.[3,17]

Scheme 1

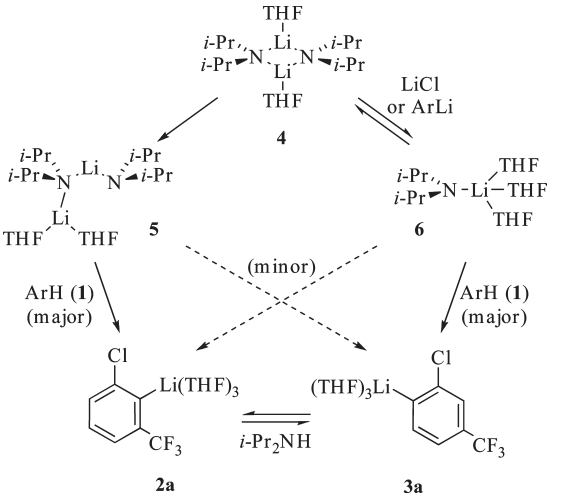

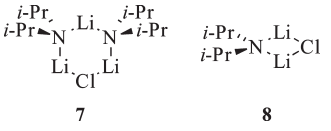

Kinetics: General Protocols. Acceleration of ortholithiations by as little as 0.01 mol % LiCl (*1.0 ppm*) demands preparation of rigorously LiCl-free LDA from lithium metal and isoprene. The solid LDA was subsequently recrystallized from hexanes.[3] Exogenous LiCl was generated in situ from $Et_3N\cdot HCl$.[18] Et_3N is a poor ligand[19] that has no effect on LDA structure or reactivity.

The disappearance of arene **1** is most conveniently followed using in situ IR spectroscopy (1325 cm^{-1}).[20] ^{19}F NMR spectroscopy was used to follow **1** (δ −62.21 ppm), **2** (δ −61.71 ppm), and **3** (δ −60.90 ppm) concurrently. The initial rates of metalation[21] were obtained from the first derivative of a polynomial fit to data from 0−5% conversion.[22] On several occasions the reaction temperature was raised to −65 °C (as noted) to avoid protracted reaction times.

Uncatalyzed Ortholithiation: Rate-Limiting Deaggregation. Let us first examine the mechanism of the uncatalyzed metalation. Monitoring the metalation of **1** at early conversion, measuring the rates before the onset of autocatalysis, reveals a rate-limiting deaggregation of dimer **4**. Thus, a plot of initial rate versus arene **1** concentration shows a clear zeroth-order dependence consistent with the absence of arene **1** in the rate-limiting

dx.doi.org/10.1021/ja200906z |*J. Am. Chem. Soc.* 2011, 133, 7135–7151

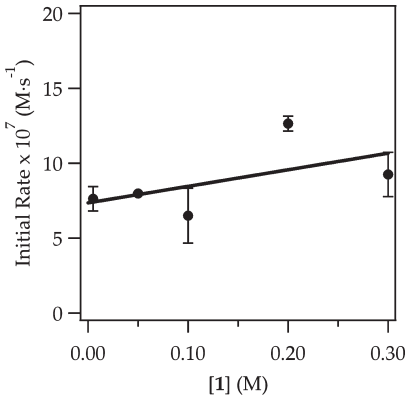

Figure 3. Plot of initial rate vs [**1**] (initial arene concentration) for the ortholithiation of **1** with LDA (0.10 M) in THF (12.2 M) at −78 °C measured by IR spectroscopy. The curve depicts an unweighted least-squares fit to $y = a[\mathrm{ArH}] + b$. [$a = (9 \pm 1) \times 10^{-7}$, $b = (7 \pm 8) \times 10^{-9}$.]

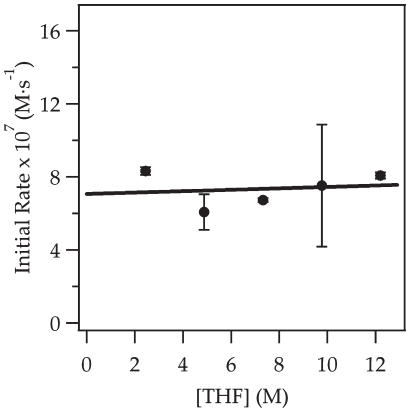

Figure 4. Plot of initial rate versus [THF] in hexanes for the ortholithiation of **1** (0.050 M) by LDA (0.10 M) at −78 °C measured by IR spectroscopy. The curve depicts an unweighted least-squares fit to $y = a[\mathrm{THF}] + b$. [$a = (7 \pm 1) \times 10^{-7}$, $b = (3.9 \pm 0.1) \times 10^{-9}$.]

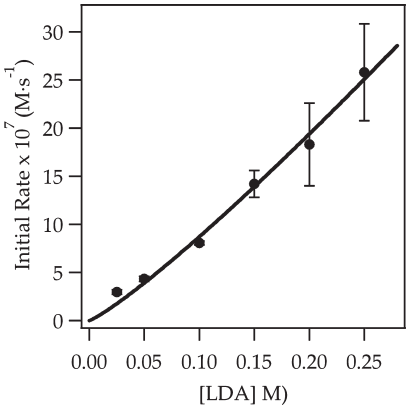

Figure 5. Plot of initial rate versus [LDA] in THF (12.2 M) for the ortholithiation of **1** (0.050 M) at −78 °C measured by IR spectroscopy. The curve depicts an unweighted least-squares fit to $y = a[\mathrm{LDA}]^n$. [$a = (1.2 \pm 0.2) \times 10^{-5}$, $n = (1.16 \pm 0.09)$.]

step (Figure 3).[23] The initial rates are independent of THF concentration (Figure 4) and display an approximate first-order dependence (1.16 ± 0.09 order) on LDA concentration (Figure 5).[24,25] Isotopic labeling studies (below) confirm post-rate-limiting proton transfer.

To simplify mechanistic discussions, we introduce the following shorthand: A = an LDA subunit, S = THF, ArH = arene, and ArLi refers to aryllithiums **2** and **3** collectively. By example, A_2S_2 corresponds to disolvated LDA dimer **4**. The rate data are consistent with the idealized[26] rate law in eq 2. The generic mechanism described by eq 3 reduces to eq 4 because the trapping step is efficient ($k_2[\mathrm{ArH}] \gg k_{-1}$). Curiously, previous studies of 1,4-additions of LDA to unsaturated esters revealed a rate-limiting deaggregation of dimer **4**,[3] but in those studies the rate-limiting step involved a *tris*olvated-dimer-based transition structure, $[A_2S_3]^{\ddagger}$. The existence of $[A_2S_3]^{\ddagger}$ constitutes the first of several observations suggesting that $[A_2S_2]^{\ddagger}$ is the rate-limiting transition structure en route to only *partial* deaggregation. DFT computations indicate that facile solvent reorganization is followed by the formation of open dimer **5** via a quite reasonable transition structure **9** (eq 5).[27]

$$-\frac{\mathrm{d}[\mathrm{ArH}]}{\mathrm{d}t} = k[A_2S_2][S]^0[\mathrm{ArH}]^0 \quad (2)$$

$$A_2S_2 \underset{k_{-1}}{\overset{k_1}{\rightleftharpoons}} [A_2S_2{*}] \xrightarrow{k_2[\mathrm{ArH}]} \mathrm{ArLi} \quad (3)$$

$$A_2S_2 \xrightarrow{k_1} [A_2S_2]^{\ddagger} \quad (4)$$

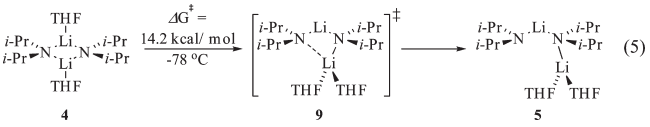

(5)

Uncatalyzed Ortholithiation: Kinetic Isotope Effects. Deuterium labeling studies confirm that the critical proton transfer (still measured at early conversion) is post-rate-limiting. The analysis was carried out using ^{19}F NMR spectroscopy and is summarized in Scheme 2. By first focusing on the unlabeled substrate (**1**) and monodeuterated substrates (**1**-2-*d* and **1**-6-*d*), we noted that the rates of disappearance of the three isotopomers are indistinguishable (±5%) despite the suppression of specific pathways. Such equivalent intermolecular isotope effects[28,29] are consistent with post-rate-limiting proton (deuterium) transfers. The ratios of rate constants corresponding to isotopically sensitive (but post-rate-limiting) branch points ($k_{H(2)}/k_{H(6)}$, $k_{D(2)}/k_{H(6)}$, and $k_{H(2)}/k_{D(6)}$) were determined by measuring the respective **2**/**3** ratios at early conversion using ^{19}F NMR spectroscopy. The regioselectivities make intuitive sense: deuteration at C2 (**1**-2-*d*) markedly promotes metalation at C6 (**2**:**3** = 1:18), whereas deuteration at C6 (**1**-6-*d*) promotes metalation at C2 (**2**:**3** = 34:1). The intramolecular isotope effects[28,29] corresponding to $k_{H(2)}/k_{D(2)}$ and $k_{H(6)}/k_{D(6)}$ were calculated according to eqs 6 and 7 and found to be substantial and inequivalent.[30]

$$k_{H(2)}/k_{D(2)} = (k_{H(2)}/k_{H(6)})(k_{H(6)}/k_{D(2)}) = 31 \quad (6)$$

$$k_{H(6)}/k_{D(6)} = (k_{H(6)}/k_{H(2)})(k_{H(2)}/k_{D(6)}) = 19 \quad (7)$$

The behavior of doubly deuterated arene **1**-2,6-d_2 diverges from that of the other three substrates and offers an interesting window into the mechanism.[31] The curvatures exhibited by the

dx.doi.org/10.1021/ja200906z |*J. Am. Chem. Soc.* 2011, 133, 7135–7151

Scheme 2

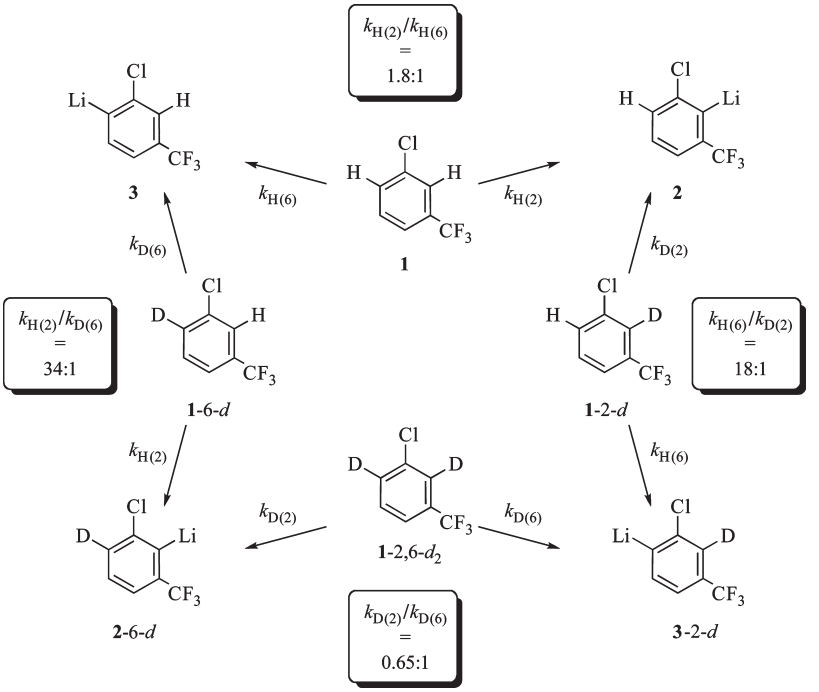

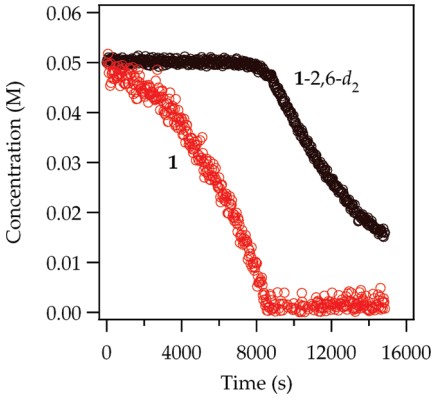

Figure 6. Competitive ortholithiation of **1** (0.050 M) and **1**-2,6-d_2 (0.050 M) with LDA (0.10 M) in THF (12.2 M) at −78 °C monitored by IR spectroscopy.

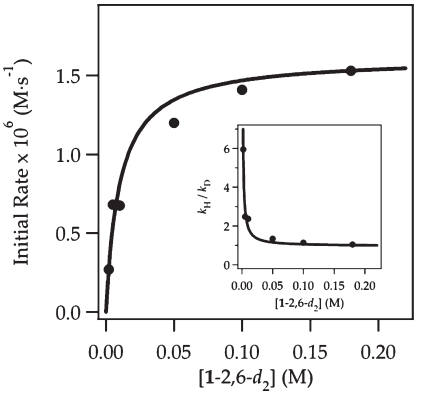

Figure 7. Plot of initial rate versus **1**-2,6-d_2 for the ortholithiation of **1**-2,6-d_2 by 0.10 M LDA in 12.2 M THF at −78 °C measured by IR spectroscopy. The curve depicts an unweighted least-squares fit to a first-order saturation function: $-\Delta[ArH]/\Delta t|_{t=0} = (a[ArH])/(1 + b[ArH])$ where ArH is **1**-2,6-d_2. The ratio a/b was constrained to 1.6×10^{-6} M s^{-1} to ensure saturation at the initial rate of **1** (1.6×10^{-6} M s^{-1}). [b = $(2.62 \pm 0.08) \times 10^{-6}$.]

decays are highly dependent on arene concentration. At high concentration (0.10 M) we observe downward curvature characteristic of autocatalysis. As the concentration decreases, the downward curvature gives way to upward curvature that becomes exponential at <0.005 M, which is expected for first-order arene dependencies.

The upward curvature suggests that deuteration causes the metalation to become at least partially rate limiting.[32] Moreover, the initial metalation rate at 0.050 M **1**-2,6-d_2 is approximately 3-fold slower than that of the other three isotopomers (eq 8), showing that the metalation rate has an attenuated but detectable isotopic sensitivity. To understand the origins of this partial rate limitation we return to eq 3. A rate-limiting deaggregation demands that the fleeting intermediate denoted as $A_2S_2^*$ (suggested computationally to be open dimer **5**) be trapped efficiently by ArH ($k_2[ArH] \gg k_{-1}$).

The much slower metalations of **1**-2,6-d_2 cause deuterium transfer to become partially rate limiting ($k_2[\mathbf{1}\text{-}2,6\text{-}d_2] \approx k_{-1}$.) The appearance of **1**-2,6-d_2 in the rate law would be accompanied by upward curvature and a partial isotope effect as observed.

Several experiments confirm that lithiation of **1**-2,6-d_2 involves only partially rate-limiting deaggregation. A competitive isotope effect measured according to eq 9 plumbs post-rate-limiting behavior akin to measuring an intramolecular isotope effect,[28] except that the competitive isotope effect involves two distinct substrates. If the intermolecular isotope effect obtained using **1** and **1**-2,6-d_2 is simply a small primary kinetic isotope effect, the

dx.doi.org/10.1021/ja200906z |*J. Am. Chem. Soc.* 2011, 133, 7135–7151

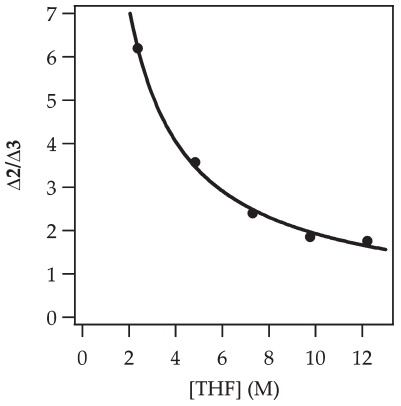

Figure 8. Ratio of relative initial rates of formation of **2** and **3**, $(\Delta\mathbf{2}/\Delta t)/(\Delta\mathbf{3}/\Delta t)$, versus [THF] in hexanes for the ortholithiation of **1** (0.050 M) by LDA (0.10 M) at −65 °C measured by ^{19}F NMR spectroscopy. The elevated temperature was used to shorten the duration of the experiments. The curve depicts an unweighted least-squares fit to $y = a[\mathrm{THF}]^n + b$. [$a = 12.5 \pm 0.8$, $n = -0.8 \pm 0.2$, and $b = 0.1 \pm 0.8$.]

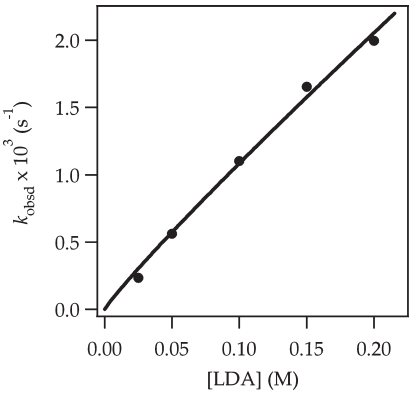

Figure 9. Plot of k_{obsd} versus [LDA] in THF (12.2 M) for the ortholithiation of **1**-2,6-d_2 (0.002 M) at −65 °C measured by ^{19}F NMR spectroscopy. The curve depicts an unweighted least-squares fit to $y = k[\mathrm{LDA}]^n$. [$k = (9 \pm 1) \times 10^{-3}$, $n = 0.92 \pm 0.06$.]

competitive isotope effect (eq 9) should be comparable. As illustrated in eq 9, the measured value is large and similar to the intramolecular isotope effects summarized in Scheme 2 and eqs 6 and 7. The crudeness of the estimate stems from technical difficulties associated with deconvoluting the IR absorbances corresponding to **1** and **1**-2,6-d_2 combined with measuring initial rates.[33] The decays of the isotopomers also display a highly revealing biphasic behavior (Figure 6) emblematic of post-rate-limiting competition between the two substrates.[3,6c] The different curvatures for **1** (downward) and **1**-2,6-d_2 (upward) also reflect separate stages along the reaction coordinate: ArLi autocatalyst has reached substantial concentrations as **1**-2,6-d_2 begins to react in earnest.

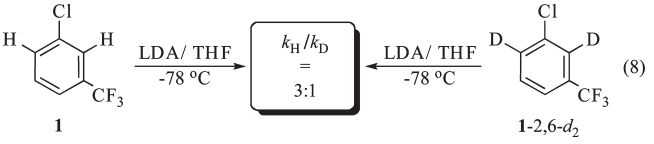

(8)

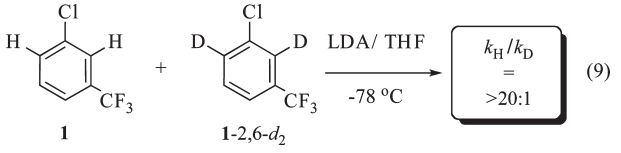

(9)

Partial rate limitation leads to a second clear prediction. If $k_2[\mathbf{1}\text{-}2,6\text{-}d_2] \approx k_{-1}$, then high **1**-2,6-$d_2$ concentrations should cause $k_2[\mathbf{1}\text{-}2,6\text{-}d_2] \gg k_{-1}$ and reduce eq 3 to eq 4. In short, high **1**-2,6-d_2 concentration would cause deaggregation to become fully rate limiting and be accompanied by a zeroth-order substrate dependence (saturation kinetics). Indeed, Figure 7 shows saturation at high **1**-2,6-d_2 concentration that is accompanied by nearly identical rates of disappearance for **1** and **1**-2,6-d_2. The curve in Figure 7 is a simple first-order saturation function, and the concentrations refer to initial concentrations. The inset in Figure 7 shows a slightly different view by plotting the intermolecular isotope effect versus **1**-2,6-d_2 concentration, which approaches unity at the high concentration limit.

Uncatalyzed Ortholithiation: Mechanisms of Proton Transfers. The regioselectivity in this reaction provides a glimpse beyond rate-limiting deaggregation, a portion of the reaction coordinate considered largely invisible to kineticists. Monitoring the initial rates of formation of aryllithiums **2** and **3** using ^{19}F NMR spectroscopy affords what one might call a *relative* rate law (eq 10). If, for example, **2** and **3** form via a single (shared) fleeting intermediate, then the regioselectivity (the post-rate-limiting branch) would be independent of LDA and THF concentrations. Indeed, the product ratios are independent of LDA concentration, showing a shared aggregation state. By contrast, although the overall metalation rates are THF-concentration independent, the product ratios show a greater tendency to form **3** at elevated THF concentration (Figure 8). A nonlinear least-squares fit shows that the metalation to form **3** requires *one* THF ligand beyond what is required for the metalation to form **2**.

$$[\mathbf{2}]/[\mathbf{3}] = c[\mathrm{ArH}]^0[\mathrm{LDA}]^0[\mathrm{THF}]^{-1} \qquad (10)$$

Metalations at the lowest concentrations of **1**-2,6-d_2, conditions in which both the curvatures and isotope effects indicate that the rate-limiting step is deuterium transfer, allowed us to probe the events following the deaggregation step. A plot of k_{obsd} vs LDA concentration (Figure 9) shows near linearity (0.92 order), indicating that the metalation of **1**-2,6-d_2 is dimer-based[23] as suspected. The corresponding plot of k_{obsd} versus THF concentration affords an altogether unexpected second-order THF dependence (Figure 10). Switching from hexane to 2,5-Me$_2$ THF as the cosolvent to maintain a more constant polarity had no effect on the observed rates, again affording a second-order THF dependence. The combined data afford the rate law in eq 11 and the mechanism in eq 12 involving tetrasolvated dimers. We hasten to add that the two terms in eq 11 (the second order affiliated with the formation of **2** and the third-order solvent affiliated with formation of **3**) and accompanying tetra- and pentasolvated terms in eq 12 do *not* derive from the measured solvent order in Figure 10 (which clearly approximates two) but rather from the relative solvent order illustrated in Figure 8 demanding differential solvation. We estimate from relative contributions of pathways leading to **2** and **3** that the measured solvent order should have measured slightly above 2.

dx.doi.org/10.1021/ja200906z |*J. Am. Chem. Soc.* 2011, 133, 7135–7151

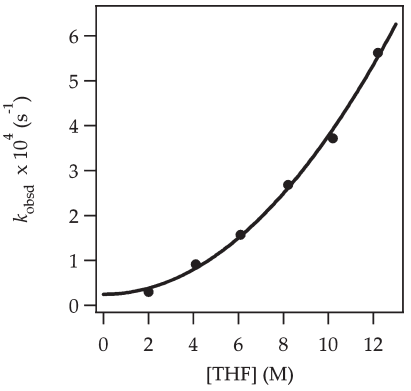

Figure 10. Plot of k_{obsd} versus [THF] in hexanes for the ortholithiation of **1**-2,6-d_2 (0.002 M) by LDA (0.050 M) at −65 °C measured by ^{19}F NMR spectroscopy. The curve depicts an unweighted least-squares fit to $y = k[\mathrm{THF}]^n + c$. [$k = (3 \pm 1) \times 10^{-6}$, $n = 2.0 \pm 0.2$, and $c = (3 \pm 1) \times 10^{-5}$.]

Concerned that we might be getting deceived by the LDA order, we examined the influence of LiCl on the metalation rates. If the rate-limiting metalation proceeds via a pre-equilibrated monomer-based pathway, then LiCl should have no effect because LiCl serves to catalyze dimer−monomer exchange (vide infra). In the event, addition of LiCl to a metalation of **1**-2,6-d_2 at low concentrations elicited a 10-fold acceleration, suggesting that the uncatalyzed and LiCl-catalyzed metalation are indeed different. Triple ions **10** and **11** are computationally viable candidates for the dimer-based reactions. Although the absolute energies of such highly ionized forms are of little value, **10** is 3.5 kcal/mol more stable than **11**.[3,34]

$$-\frac{\mathrm{d[ArH]}}{\mathrm{d}t} = k_{(2)}[\mathrm{ArD}]^1[\mathrm{A_2S_2}][\mathrm{S}]^2 + k_{(3)}[\mathrm{ArD}]^1[\mathrm{A_2S_2}][\mathrm{S}]^3 \qquad (11)$$

$$\mathrm{A_2S_2} \underset{k_{-1}}{\overset{k_1}{\rightleftharpoons}} [\mathrm{A_2S_{4/5}}] \xrightarrow{k_2[\mathrm{ArD}]} \mathrm{ArLi} \qquad (12)$$

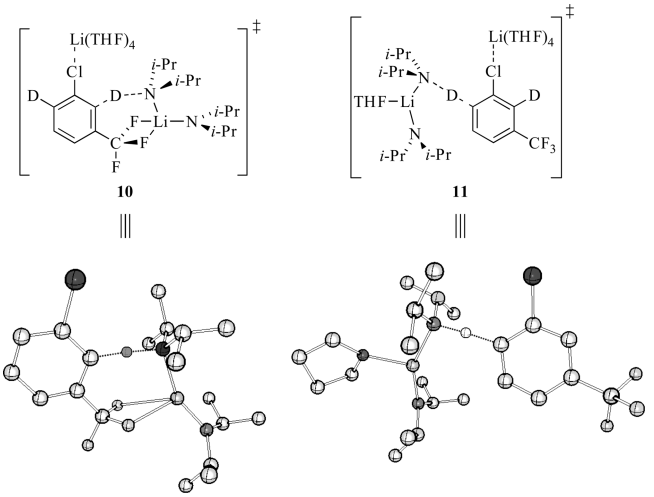

Although the data implicate tetra- and pentasolvated dimers, we also explored various di- and trisolvated-dimer-based transition structures summarized in Figure 11. (We include those leading to the unobserved regioisomeric ArLi for comparison.) All are computationally reasonable, displaying absolute activation energies of 13−18 kcal/mol. The origins of the solvent-dependent regioselectivities fall within the error of the computations.[35]

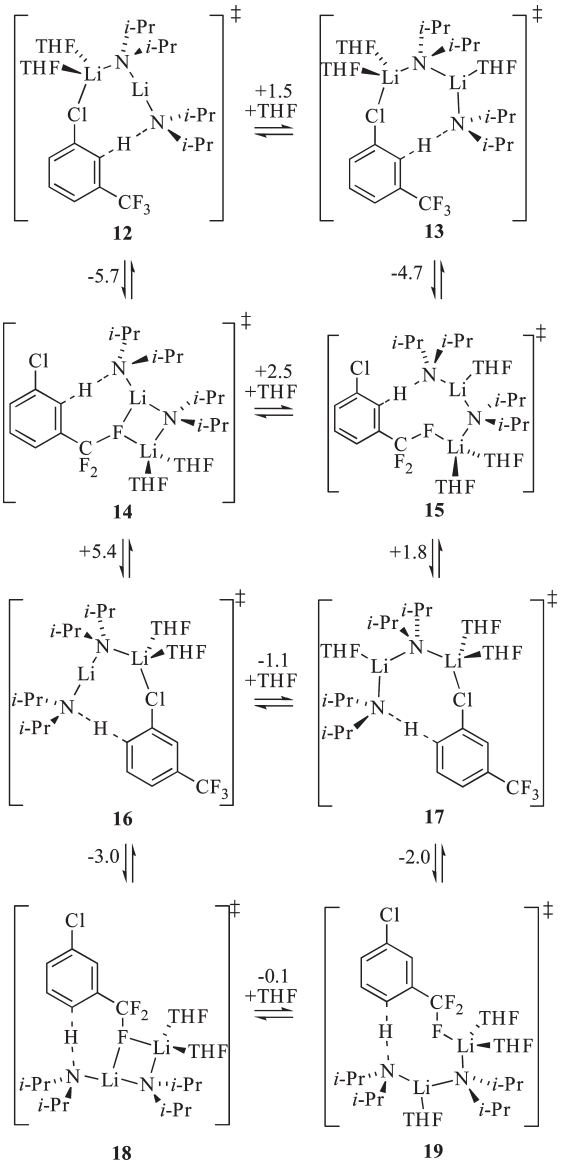

Figure 11. DFT computations [MP2/6-31G(d)//B3LYP/6-31G(d)] of dimer-based transition structures for the metalation of **1**. The free energy of activation for the formation of **12** ($\Delta G^{\ddagger}$) is 19.3 kcal/mol calculated at −78 °C. The numbers affiliated with the arrows represent the relative free energies (ΔG).

LiCl Catalysis. Traces of LiCl elicit marked rate accelerations that are accompanied by distinct upward curvatures, suggesting that LiCl catalysis brings arene **1** back into the rate law. Clean first-order decays are observed at >5 mol % LiCl (Figure 12). A plot of the initial rates versus LiCl concentration shows second-order saturation kinetics with the onset of saturation at low levels (<2.0 mol % LiCl) as noted in previous studies (Figure 13).[3,6] The saturation behavior in Figure 13 is *not* Michaelis−Menten kinetics, however, which would require stoichiometric LiCl to attain saturation.[36] It should also not be confused with the saturation kinetics noted for metalations of **1**-2,6-d_2 shown in Figure 7 (although

dx.doi.org/10.1021/ja200906z |*J. Am. Chem. Soc.* 2011, 133, 7135–7151

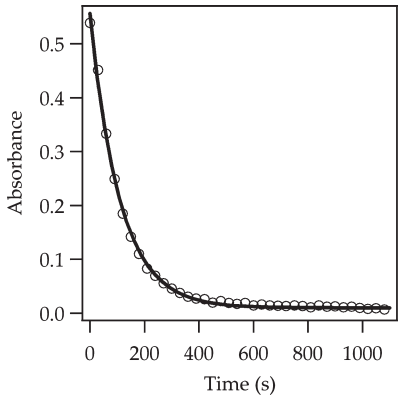

Figure 12. Representative plot of the IR absorbance of **1** (0.005 M) versus time for the ortholithiation by LDA (0.10 M) in 12.2 M THF in the presence of 5 mol % LiCl (0.005 M) at −78 °C. The curve depicts an unweighted least-squares fit to $y = Ae^{-kt}$.

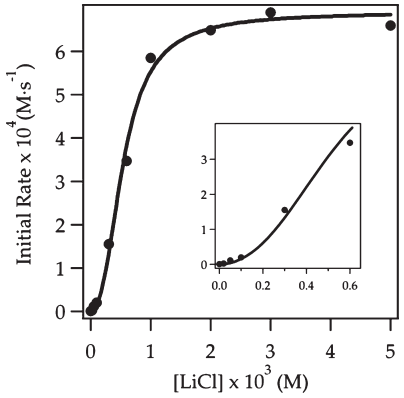

Figure 13. Plot of initial rate versus [LiCl] for the ortholithiation of **1** (0.074 M) by 0.10 M LDA in 12.2 M THF at −78 °C measured by IR spectroscopy. The inset is a magnified view of the data at low concentrations. The curve depicts an unweighted least-squares fit to eq 17. [ArH] = 0.074 M, $[A_2S_2]$ = 0.050 M, and $c = 1.0 \times 10^{-8}$. [$k_1 = (1.5 \pm 0.1) \times 10^4$, $k_{-1} = (3.2 \pm 0.4) \times 10^6$, $k_2 = 0.61 + (6 \times 10^{-4})$, and $n = 2.0 \pm 0.3$.]

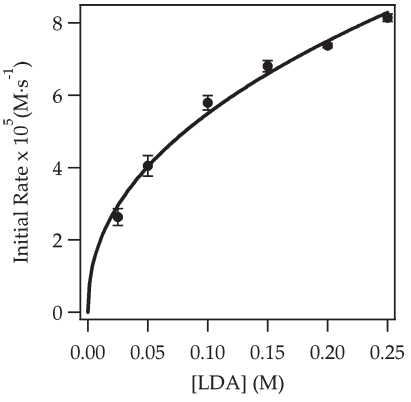

Figure 14. Plot of initial rate versus [LDA] in THF (12.2 M) for the ortholithiation of **1** (0.075 M) in the presence of 5 mol % LiCl (0.005 M) at −78 °C measured by IR spectroscopy. The curve depicts an unweighted least-squares fit to $y = a[\mathrm{LDA}]^n$. [$a = (154 \pm 9) \times 10^{-6}$, $n = 0.45 \pm 0.03$.]

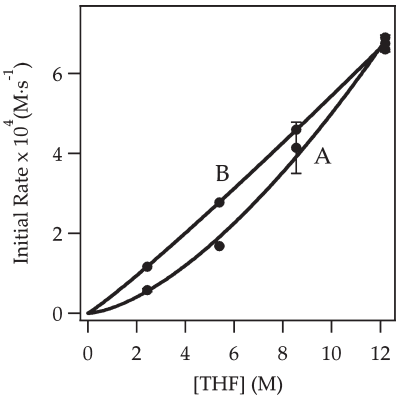

Figure 15. Plot of initial rate versus [THF] in hexanes (curve A) and 2,5-dimethyl-tetrahydrofuran (curve B) cosolvent for the ortholithiation of **1** (0.075 M) by LDA (0.10 M) in the presence of 5 mol % LiCl at −78 °C. The data were measured by IR spectroscopy. The curves depict unweighted least-squares fits to $y = a[\mathrm{THF}]^n + b$. Curve A: $a = (1.4 \pm 1.0) \times 10^{-5}$, $n = 1.6 \pm 0.3$, $b = (1.6 \pm 1) \times 10^{-5}$. Curve B: $a = (4.44 \pm 2.0) \times 10^{-5}$, $n = 1.1 \pm 0.1$, $b = (0.0 \pm 5) \times 10^{-5}$.

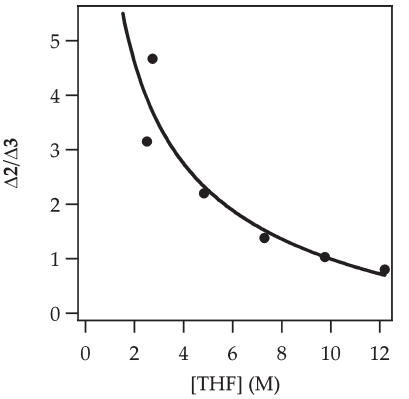

Figure 16. Plot of relative initial rate versus [THF] in 2,5-dimethyltetrahydrofuran cosolvent for the ortholithiation of **1** (0.050 M) by LDA (0.10 M) in the presence of 5 mol % LiCl at −78 °C. The concentrations of **2** and **3** were monitored by ^{19}F NMR spectroscopy. The curve depicts an unweighted least-squares fit to $y = a[\mathrm{THF}]^n + b$. [$a = 9 \pm 6$, $n = -0.94 \pm 0.21$, and $b = 0.0 \pm 0.3$.]

they are related). *LiCl catalyzes a deaggregation.* Analogous LiCl saturation behavior was observed for 1,4-additions of LDA to unsaturated esters, although the sigmoidal curvature evident at low LiCl concentrations (inset in Figure 13) that would signify a *second*-order LiCl dependence has not been observed.[3,37]

The details of the deaggregation were examined at full saturation (5.0 mol % LiCl) as follows. Ortholithiation of **1** and **1**-2,6-d_2 reveals large and equivalent standard and competitive isotope effects (eqs 13 and 14) consistent with rate-limiting proton (and deuterium) transfer. Plotting initial rates versus LDA concentration affords a generic half-order dependence implicating a dimer−monomer preequilibrium (Figure 14).[23] A plot of initial rates versus THF concentration using *hexanes* as cosolvent (Figure 15) shows a high (1.6 ± 0.3) order in THF. The curvature (a departure from a linear first-order dependence) was traced to medium effects using a now-routine protocol[38] in which the hydrocarbon is replaced with the polar[39] yet weakly coordinating[40] cosolvent, 2,5-dimethyltetrahydrofuran (Me_2THF). Holding the polarity of the medium

dx.doi.org/10.1021/ja200906z |*J. Am. Chem. Soc.* 2011, 133, 7135–7151

approximately constant afforded a THF order slightly above unity (1.1 ± 0.1 order). The mechanism (eqs 15 and 16) and rate law (eq 17) include provisions for second-order saturation by LiCl. The odd mathematical form of eq 17 stems from the quadratic equation required by the deaggregation.[3] The *c* term corresponds to the basal (uncatalyzed) rate. In the limit of full saturation, eq 17 reduces to eq 18.[41]

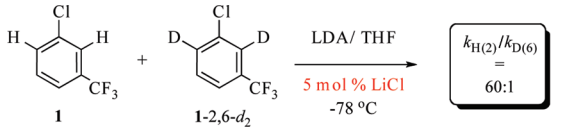

(13)

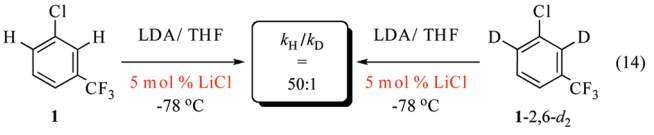

(14)

$$\frac{1}{2}A_2S_2 + S \underset{k_{-1}[\mathrm{LiCl_{total}}]^n}{\overset{k_1[\mathrm{LiCl_{total}}]^n}{\rightleftharpoons}} AS_2 \qquad (15)$$

$$AS_2 + \mathrm{ArH} \xrightarrow{k_2} [AS_2(\mathrm{ArH})]^{\ddagger} \qquad (16)$$

$$-\left.\frac{\Delta[\mathrm{ArH}]}{\Delta t}\right|_{t=0} = \frac{k_2[\mathrm{ArH}]}{4k_{-1}[\mathrm{LiCl}]^n} \times \left(\sqrt{{k_2}^2[\mathrm{ArH}]^2 + 16k_1k_{-1}[A_2S_2][\mathrm{LiCl}]^{2n}} - k_2[\mathrm{ArH}]\right) + c \qquad (17)$$

$$-\left.\frac{\Delta[\mathrm{ArH}]}{\Delta t}\right|_{t=0} = (k_1/k_{-1})^{1/2}k_2[\mathrm{ArH}][\mathrm{THF}][\mathrm{LDA}]^{0.5} \qquad (18)$$

Comparing the regioselectivity in neat THF without catalysis (**2**:**3** = 1.8:1) with that derived from LiCl catalysis (**2**:**3** = 0.85:1) shows subtle differences that are mechanistically important. Nonetheless, the regioselectivities under LiCl catalysis are, as noted for the uncatalyzed metalation, independent of LDA concentration and dependent on the THF concentration (Figure 16). In conjunction with the rate law, the results implicate an $[AS_3(\mathrm{ArH})]^{\ddagger}$ stoichiometry for the formation of **3** and an $[AS_2(\mathrm{ArH})]^{\ddagger}$ stoichiometry for the formation of **2**. We examined the selectivities using DFT computations (Figure 17). All are computationally reasonable, displaying absolute activation energies of 12−15 kcal/mol.[35] Disolvated monomer-based transition structure **21** and the corresponding trisolvate **24** are the most favorable, consistent with both the rate data and THF-dependent regioselectivities.

Autocatalysis. Autocatalysis is easily detected as downward curvature in plots of arene **1** versus time (Figure 1B).[42,43] What makes detailed studies so challenging is that (1) **2** and **3** display different autocatalytic activities, (2) autocatalysis diverts dimer-based metalations prevalent in the absence of catalysis to monomer-based metalations, (3) the dimer- and monomer-based metalations display inherently different regioselectivities, and (4) an equilibration pathway superimposed on the autocatalysis converts **3** to **2**.

The task of untangling the role of autocatalysis began with a routine control experiment to confirm its existence. After a kinetic run using 0.10 M LDA and 0.010 M arene **1** in neat THF, the IR baseline was zeroed and a second aliquot of **1** added (Figure 18).

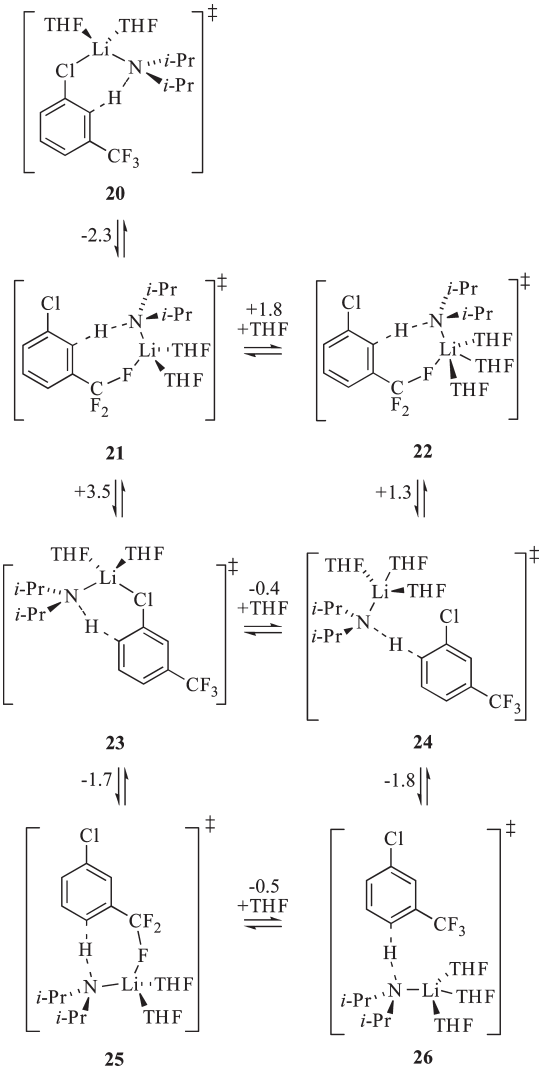

Figure 17. DFT computations [MP2/6-31G(d)//B3LYP/6-31G(d)] of monomer-based transition structures for the metalation of **1**. The free energy of activation for the formation of **20** ($\Delta G^{\ddagger}$) is 14.5 kcal/mol calculated at −78 °C. The numbers affiliated with the arrows represent the relative free energies (ΔG).

The loss of arene displays a distinct acceleration accompanied by substantially greater upward curvature (loss of downward curvature). Autocatalysis by ArLi (**2** and **3**) is analogous to the 100-fold more efficient catalysis by LiCl. Of particular note, the regioselectivities for the ArLi- and LiCl-catalyzed metalations are indistinguishable (**2**:**3** = 0.85:1) and different from the 1.8:1 ratio observed for the uncatalyzed metalation. Moreover, plotting the initial rates versus ArLi concentration (Figure 19) shows saturation kinetics analogous to that observed for LiCl (Figure 13) but at much higher ArLi concentrations. The data shown in Figure 19 was generated using regioisomer **2**-6-*d* because it was easily generated in 95% regioisomeric purity from **1**-6-*d* by exploiting the isotope effect to direct the metalation. Comparing the efficacy of catalysis using **2**-6-*d* (generated in situ from **1**-6-*d*) to the catalysis elicited by **3**-2-*d* (generated in situ from **1**-2-*d*), we found that regioisomer **2** is 6-fold more effective than **3** as an autocatalyst.

Mechanism of Equilibration. Conversion of ArLi **3** to **2** is observed over the course of the metalations and is readily effected

dx.doi.org/10.1021/ja200906z |*J. Am. Chem. Soc.* 2011, 133, 7135–7151

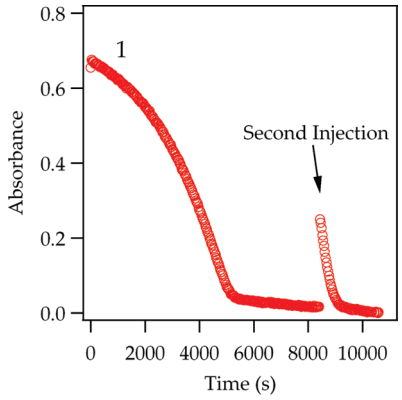

Figure 18. Representative plot showing absorbance of arene **1** vs time for the ortholithiation of **1** (0.010 M) with LDA (0.10 M) in THF (12.20 M) at −78 °C. After completion of the reaction a second aliquot of **1** (0.005 M) was injected.

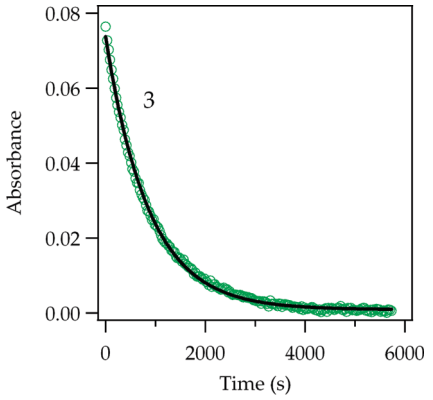

Figure 20. Representative plot of absorbance of **3** (0.050 M, 1154 cm^{-1}) versus time for isomerization by *i*-Pr_2NH (0.31 M) in 12.2 M THF at −78 °C. The curve depicts an unweighted least-squares fit to $y = Ae^{-kt}$.

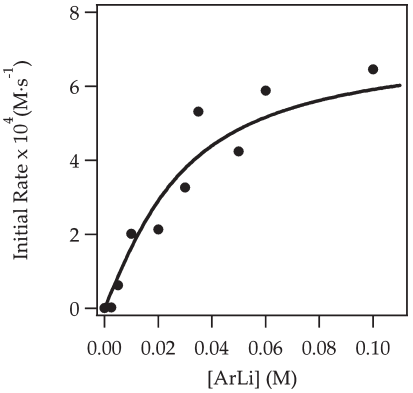

Figure 19. Plot of initial rate versus aryllithium **2**-6-*d* for the ortholithiation of **1** (0.075 M) by 0.10 M LDA in 12.2 M THF at −78 °C measured by IR spectroscopy. Aryllithium **2** was generated from **1**-6-*d* with 1 equiv LDA at −40 °C prior to injection **1**. The curve depicts an unweighted least-squares fit to a simple first-order saturation function: $-\Delta[ArH]/\Delta t|_{t=0} = (k_1k_2[A_2S_2][ArH])/(k_{-1} + k_2[ArH])$ where [ArH] = 0.075 M, $[A_2S_2]$ = 0.050 M. k_2 was constrained to the same value corresponding to lithium chloride saturation (see Figure 13). [k_1 = (0.18 ± 0.02); k_{-1} = (1.97 ± 0.01) × 10^9.]

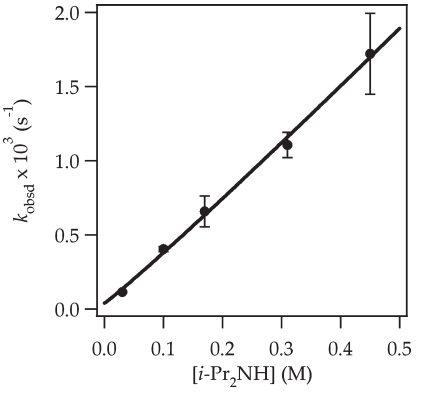

Figure 21. Plot of k_{obsd} vs [*i*-Pr_2NH] for the isomerization of **3** (0.050 M) to **2** in 12.2 M THF at −78 °C measured by IR spectrocopy. The curve depicts an unweighted least-squares fit to $y = k[i\text{-}Pr_2NH]^n + c$. [$k$ = (3.8 ± 0.3) × 10^{-3}, n = 1.1 ± 0.1, c = (2 ± 1) × 10^{-5}.]

through gentle warming. The equilibration is accelerated by added *i*-Pr_2NH, which was anticipated from rate studies of a reaction requiring an analogous equilibration.[5] To study the mechanism in detail, we generated less stable regioisomer **3** from **1** in 20:1 selectivity using LiTMP. Equilibration during the ortholithiation is negligible because the highly hindered *N,N,N′,N′*-tetramethylpiperidine byproduct does not mediate the exchange. Subsequent addition of *i*-Pr_2NH initiates the conversion of **3** to **2**. The decay of ArLi **3** fits a first-order function (Figure 20). The pseudo-first-order rate constants show a first-order dependence on *i*-Pr_2NH (Figure 21) and a zeroth-order dependence on THF. The idealized[26] rate law (eq 19) in conjunction with the assigned resting state of **3** as trisolvate **3a** is consistent with the generic mechanism in eqs 20 and 21. The proton transfer is necessarily *partially* rate limiting in that the fleeting arene partitions to an ≈1:1 mixture of **2** and **3**. It is satisfying that transition structure $[(ArLi)(THF)_3(i\text{-}Pr_2NH)]^{‡}$ for the protonation of **2** is stoichiometrically the same as the transition structure $[(i\text{-}Pr_2NLi)(THF)_3(ArH)]^{‡}$ for metalation because the principle of microscopic reversibility[44] demands that they be the same transition structure.

$$-\frac{d[\mathbf{3}]}{dt} = k'[\mathbf{3}][i\text{-}Pr_2NH][THF]^0 \quad (19)$$

$$\underset{(3)}{ArLiS_3} + i\text{-}Pr_2NH \rightarrow [ArLiS_3(i\text{-}Pr_2NH)]^{‡} \rightarrow ArH + [AS_3] \quad (20)$$

$$ArH + [AS_3] \xrightarrow{fast} \mathbf{2} + \mathbf{3} \quad (21)$$

Mechanistic Hypothesis and Numeric Integrations. Rate and mechanistic studies were pieced together to form the mechanistic hypothesis shown in Scheme 1, which has been reformulated as Scheme 3 and described by the affiliated differential equations in eqs 22−28. (A_2* represents an activated LDA dimer whereas $ArLi_{(2)}$ and $ArLi_{(3)}$ denote aryllithiums **2** and **3**.) We have taken some liberties with the depiction of the model in Scheme 3 to optimize the visual presentation. Although the role of solvent has been elucidated for a number of steps, it is not germane to the numerical fits and has been omitted for clarity. We depict the critical autocatalytic step by affiliating k_2 and k_{-2} with autocatalyst ArLi (either **2** or **3**); it is

dx.doi.org/10.1021/ja200906z |*J. Am. Chem. Soc.* 2011, 133, 7135–7151

described numerically in the differential equations based on the equilibrium

$$A_2 + ArH \rightleftharpoons A + ArLi + i\text{-}Pr_2NH$$

ArLi generically stands for $ArLi_{(2)}$ and $ArLi_{(3)}$. Because $ArLi_{(3)}$ is 6 times less catalytically active than $ArLi_{(2)}$, its rate contribution is scaled accordingly in the curve fit. (We avoid treating the two autocatalysts separately.) The equilibria in Scheme 3 are unbalanced to minimize clutter. The differential equations, by contrast, are all fully balanced to provide a valid mathematical description. Representative results from best-fit numerical integrations are illustrated in Figure 1.

$$\frac{d[ArH]}{dt} = -k_3[A_2{*}][ArH] - k_4[A_2{*}][ArH] - k_5[A][ArH] - k_6[A][ArH] \quad (22)$$

$$\frac{d[A_2]}{dt} = -k_1[A_2] + k_{-1}[A_2{*}] - k_2[A_2]([ArLi_{(2)}] + 1/6[ArLi_{(3)}]) + k_{-2}[A]^2([ArLi_{(2)}] + 1/6[ArLi_{(3)}]) + 1/2k_3[A_2{*}][ArH] + 1/2k_4[A_2{*}][ArH] \quad (23)$$

$$\frac{d[A]}{dt} = 2k_2[A_2]([ArLi_{(2)}] + 1/6[ArLi_{(3)}]) - 2k_{-2}[A]^2([ArLi_{(2)}] + 1/6[ArLi_{(3)}]) - k_5[A][ArH] - k_6[A][ArH] \quad (24)$$

$$\frac{d[A_2{*}]}{dt} = k_1[A_2] - k_{-1}[A_2{*}] - k_3[A_2{*}][ArH] - k_4[A_2{*}][ArH] \quad (25)$$

$$\frac{d[ArLi_{(2)}]}{dt} = k_3[A_2{*}][ArH] + k_5[A][ArH] + k_7[ArLi_{(3)}][i\text{-}Pr_2NH] - k_{-7}[ArLi_{(2)}][i\text{-}Pr_2NH] \quad (26)$$

$$\frac{d[ArLi_{(3)}]}{dt} = k_4[A_2{*}][ArH] + k_6[A][ArH] + k_{-7}[ArLi_{(2)}][i\text{-}Pr_2NH] - k_7[ArLi_{(3)}][i\text{-}Pr_2NH] \quad (27)$$

$$\frac{d[i\text{-}Pr_2NH]}{dt} = k_3[A_2{*}][ArH] + k_4[A_2{*}][ArH] + k_5[A][ArH] + k_6[A][ArH] \quad (28)$$

DISCUSSION

Summary. Metalation of arene **1** by LDA in THF at −78 °C (eq 1) joins a growing list of LDA-mediated reactions in which rates of aggregate exchanges dictate reactivity and in which autocatalysis and catalysis by exogenous lithium salts are prominent. The results can be understood in the context of Scheme 1 with amplification in Scheme 4. Under conditions in which lithium salt catalysis is absent (metalations of **1** at early conversion using rigorously LiCl-free LDA) the rate-limiting step involves LDA deaggregation via a disolvated-dimer-based transition structure. DFT computations are consistent with dimer-based transition structure **9** to form open dimer **5** (eq 5). Open dimers are prominent in many of our discussions of LDA-mediated reactions.[23,27]

The post-rate-limiting proton transfers manifest a mechanistic bifurcation in which the critical metalation steps proceed via

Scheme 3

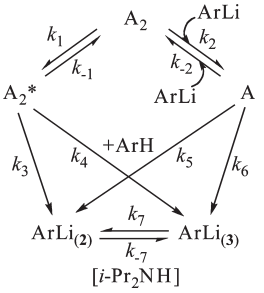

differentially solvated dimers. We seriously considered di- and trisolvated dimers, and DFT computations were supportive (Figure 11). Rate studies of **1**-2,6-d_2, however, implicated tetra- and pentasolvated dimers. To explain the high solvent orders we turned to triple-ion-based transition structures **10** and **11**, which were shown to be computationally viable. The result is that the *rate* of metalation is THF independent but the *regioselectivity* shows a distinct THF dependence.

Lithium salts catalyze the deaggregation of LDA by diverting metalations through monomer-based pathways. LiCl catalysis, for example, causes large (100-fold) accelerations and affords concentration dependencies and isotope effects consistent with di- and trisolvated-monomer-based metalations and rate-limiting proton transfers. Computational studies support di- and trisolvated-monomer-based transition structures **21** and **24** (Scheme 4), but others are plausible as well (Figure 17).

In the absence of LiCl, autocatalysis by **2** and **3** that form during the reaction elicits acceleration as the reaction proceeds (Figure 1B). Autocatalysis appears to divert the reaction through the same monomer-based pathways as those shown in Scheme 4. This conclusion derives support from regioselectivities that suggest a commonality of intermediate(s) with LiCl-catalyzed metalation. Moreover, **2** is 6-fold more autocatalytically active than is isomer **3**. Both pale in comparison with LiCl, however.

Diisopropylamine formed during the reaction slowly equilibrates regioisomers **2** and **3**. Such equilibrations are well-known,[4,5] and participation by diisopropylamine has been documented.[4i,j] Detailed studies of such an equilibration appear to have been reported in only one instance.[5] The nearly quantitative formation of **2** at equilibrium restricted rate studies to the unidirectional conversion of **3** to **2**. The conversion is shown to be the microscopic reverse of the monomer-based metalation in Scheme 4, proceeding via trisolvated-monomer-based transition structure **24**. It is *not* a particularly bold assertion that the protonation of **2** to give **1**, although kinetically invisible to us, involves the microscopic reverse of the metalation via disolvate **21**.

The independent pieces assemble to afford the mechanistic scenario summarized in Scheme 1. Additional insights about the role of solvation as well as steps that follow rate-limiting formation of open dimer **5** are not included in Scheme 1. The mechanism was reduced to the mathematically tractable model summarized in Scheme 3 and described by differential eqs 22-28. Best-fit numerical integrations are illustrated in Figure 1. On the one hand, the mechanistic model is not uniquely defined by the data; there are minor mechanistic variants that fit the data equally

Scheme 4

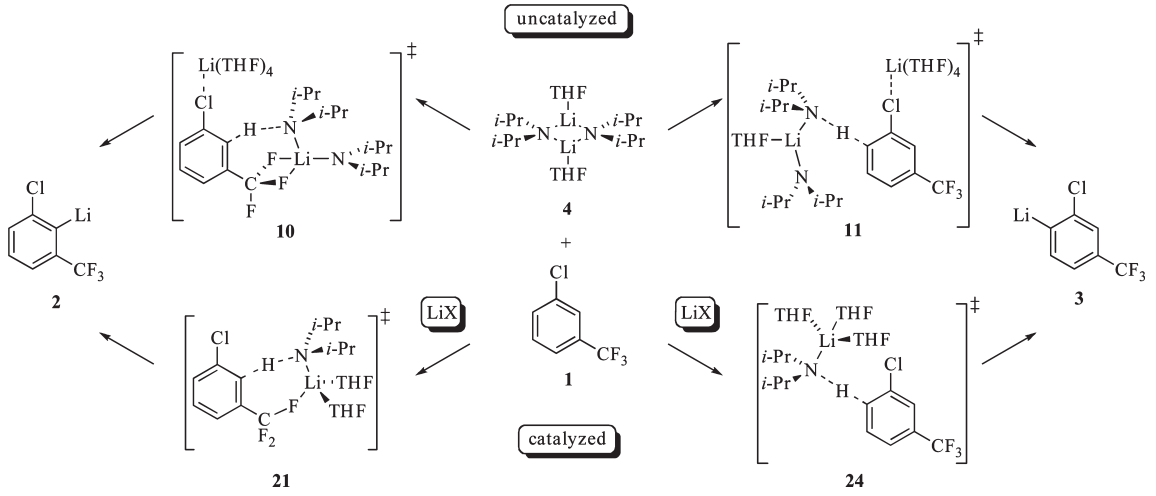

Scheme 5

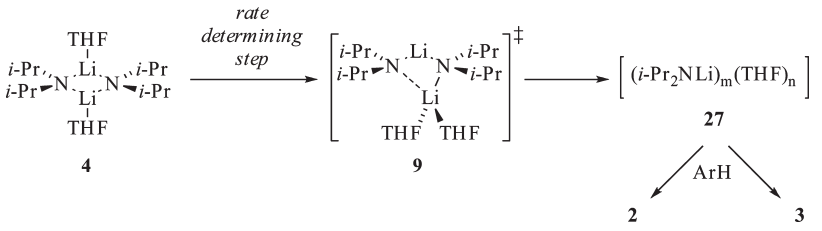

well. Nonetheless, the quality of the fits shows *consistency* with the proposed mechanism.

Regioselectivities. The regioselectivities of the metalations are highly sensitive to reaction conditions as underscored in Figures 1 and 2. A number of underlying factors are at play. In the absence of salt-catalyzed deaggregation, the metalations show a modest bias toward **2** that approaches 7:1 selectivity at low THF concentration (Figure 8), a bias that derives from the dimer-based metalations in Scheme 4. Autocatalyzed or LiCl-catalyzed metalations promote the formation of **3**, moreso at high THF concentrations, owing to the monomer-based pathways. As the reactions proceed to full conversion, however, the equilibration becomes dominant, obscuring the kinetic selectivity and affording exclusively **2** in the limit of long reaction times.

The kinetically controlled regioselectivity appears to be dominated by steric effects with contributions from an eclectic mix of directing effects. Solvating lithium cations can be sterically very demanding.[10] Not surprisingly, therefore, both dimer- and monomer-based metalations of **1** to form **2** require lower solvation numbers than do the analogous metalations to form regioisomer **3**. Coordinating effects are also complex, however. Computations show viable transition structures with lithiums ligated by trifluoromethyl and chlorine and even with no ligation by substrate whatsoever. A natural tension arises between the tendency to maximally solvate lithium with strongly coordinating solvent and the tendency to coordinate the ortho-directing moieties.[45]

Peering Beyond Rate-Limiting Steps. A rate-limiting LDA deaggregation may seem to constitute an opaque wall that renders the structures of fleeting intermediates and the mechanisms of proton transfers invisible (Scheme 5). This is incorrect. Admittedly, the intermolecular isotope effect, the influence of isotopic substitution on the reaction rate, will be unity if the proton transfer occurs after the rate-limiting step. By contrast, intramolecular isotope effects, isotope effects measured by a competition for abstraction between hydrogen and deuterium within the same molecule, will reflect the isotopic sensitivity of the post-rate-limiting metalation in the product distribution.[29] The isotope effects illustrated in Scheme 2 offer excellent examples: isotopically *insensitive* rates are accompanied by large isotopic biases in the regioselectivity. Purists might argue that these are not truly intramolecular isotope effects because they lack an explicit symmetry equivalence of the sites containing hydrogen–deuterium labels.[29] Nonetheless, solving eqs 6 and 7 affords the deconvoluted k_H/k_D values. (As an aside, it would be a mistake to get excited about isotope effects that exceed 30; they are common for ortholithiations using both LDA and *n*-BuLi.)[46]

The concept behind intramolecular isotope effects also applies to competitive isotope effects in which two isotopically distinct substrates are competed. In this experiment, comparing **1** and **1**-2,6-d_2 (eq 9) reveals a large competitive isotope effect comparable to the values in Scheme 2, confirming that the post-rate-limiting metalation is isotopically sensitive. Of particular note, the accompanying biphasic kinetics (Figure 6), in which the less reactive isotopomer metalates only after the protio form has been consumed, is highly characteristic of a post-rate-limiting branch point.[3]

Details of post-rate-limiting metalations are also reflected in their condition-dependent regioselectivities. We found, for example, that the proportions of **2** and **3** are LDA concentration

dx.doi.org/10.1021/ja200906z |*J. Am. Chem. Soc.* 2011, 133, 7135–7151

Scheme 6

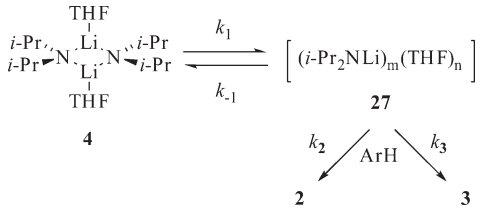

Scheme 7

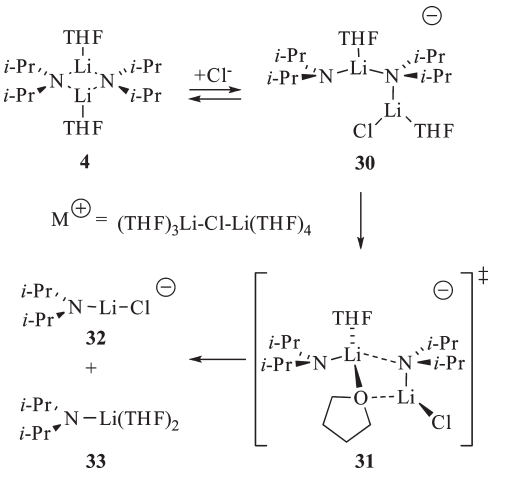

independent but show a distinct THF dependence (a preference for **3** over **2** at high THF concentration) that corresponds to transition structures differing by a single THF ligand. The relative stoichiometries of the transition structures leading to **2** and **3** are described by eq 10. Being unaware of formal nomenclature, we refer to eq 10 as a *relative rate law*. The information in eq 10 was critical for developing the mechanistic model describing the differentially solvated triple-ion-based transition structures in Scheme 4.

An altogether different strategy to observe post-rate-limiting behavior is simply to shift the rate-limiting step. Let us slightly reformulate the mechanistic scenario as Scheme 6. In the most general terms, rate limitation is determined by the relative tendency of intermediate **27** to return to starting material versus proceed to product as described by the critical ratio $(k_2 + k_3)[\mathrm{ArH}]/k_{-1}$. Deaggregation is rate limiting when the metalation by **27** is fast relative to its return to the resting state of LDA: when $(k_2 + k_3)[\mathrm{ArH}]/k_{-1} \gg 1$. By contrast, metalation becomes rate limiting when putative intermediate **27** is formed as a fully established equilibrium: $(k_2 + k_3)[\mathrm{ArH}]/k_{-1} \ll 1$.

Thus, the metalation can be brought into view by (1) increasing the rate of reaggregation, or (2) decreasing the rate of metalation. As an example of the former, LiCl-catalyzed dimer–monomer exchange causes proton transfer to become rate limiting. LiCl-catalyzed reaggregation, the accelerated back reaction in eq 15, causes the rate-limiting step to shift to proton transfer. Standard kinetic methods showed that the LiCl-catalyzed metalations proceed via di- and trisolvated-monomer-based transition structures described computationally as **21** and **24** (Scheme 4).

The alternative strategy of slowing the metalation is achieved using deuteration. As noted above, **1**-2,6-d_2 showed an isotope effect consistent with a metalation that is partially rate limiting. Partially rate-limiting steps occur when the highest barriers are also of nearly equal energy.[32] Enzymology is rich with examples, presumably because evolutionary pressures relentlessly pushed down barriers in the quest for rate efficiency.[47] Through careful control of arene concentration, the critical $(k_2 + k_3)[\mathrm{ArD}]/k_{-1}$ (such that ArD is **1**-2,6-d_2) could be shifted to produce rate-limiting deaggregation at high ArD concentration and rate-limiting metalation at low concentrations. The two limiting behaviors are seen in the saturation behavior depicted in Figure 7. By determining the rate law under conditions of rate-limiting deuterium transfer, we were able to show what we had only suspected throughout the duration of this mechanistic study: metalations of **1** in the absence of salt catalysts occur via dimers, not via monomers. The high order in THF implicating tetra- or higher-solvated dimers caught us completely by surprise. Transition structures **10** and **11** based on triple ions[34] moved to center stage rather abruptly.

Mechanism of LiCl Catalysis. LiCl influences the reaction rate by catalyzing the conversion of LDA dimer **4** to highly reactive LDA monomer,[9] and the quantities of LiCl required to attain full equilibration are stunningly small (<1.0 mol %; 1.0 ppm). Such catalysis has been observed previously, but the second-order saturation behavior evident in Figure 13 (see inset) was not observed.[6] Our ongoing struggle to understand the details of LiCl catalysis is acute because LiCl exists exclusively as a mixture of mixed aggregates **7** and **8** at such low concentrations,[3,17] and we do not know the fate of **7** and **8** under the reaction conditions. Let us make the seemingly plausible supposition, however, that the second order derives from a catalyzed deaggregation involving a transition structure of stoichiometry $[(i\text{-Pr}_2\mathrm{NLi})_2(\mathrm{LiCl})_2]^{\ddagger}$ (mixed tetramer).

We envision two fleeting intermediates that account for the catalysis and the accompanying second-order dependence on LiCl concentration. The first is ladder **28**, which has ample precedent in structural lithium amide chemistry.[48,49] The dissociation of LDA monomer from **28** (eq 29) has an energetic appeal because **28** would require dissociation of only one monomer rather than dissociating *two* high energy monomers from a dimer. The remaining three-rung ladder, **29**, could be loosely considered a leaving group.

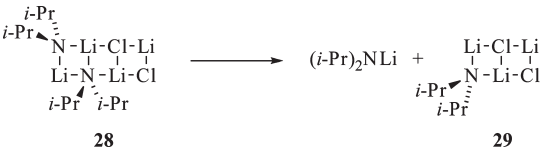

(29)

Triple ions offer an even more provocative vehicle for deaggregating LDA dimer (Scheme 7). One could view chloride ion as simply a dipolar ligand, possibly akin to a sterically unhindered hexamethylphosphoramide analogue. Ongoing computational and spectroscopic studies show that LiCl catalyzes subunit exchanges in LDA dimers.[6] Computations archived in Supporting Information show **30** to be a minimum and transition structure **31** to be only 5 kcal/mol higher energy than **30**. Adduct **30** is structurally similar to a halide adduct tentatively assigned spectroscopically.[50] Moreover, the Li–Cl–Li cationic triple ion fragment is well precedented[51] and is computationally preferred relative to the simple lithium counterion.[52] (The heptasolvation of the $(\mathrm{THF})_3\mathrm{Li–Cl–Li}(\mathrm{THF})_4$ counterion is odd, but it is the preferred form computationally.) X–Li–X anionic triple ion fragments analogous

dx.doi.org/10.1021/ja200906z | *J. Am. Chem. Soc.* 2011, 133, 7135–7151

Scheme 8

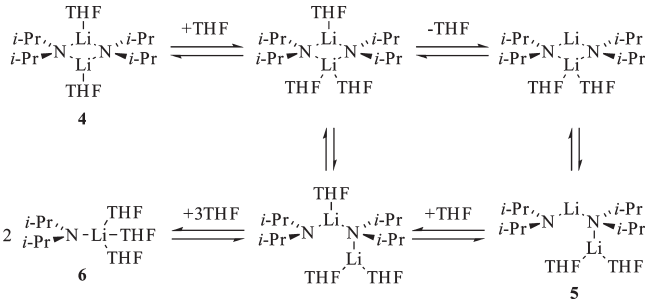

to **32** are also well documented.[34] The bridging THF in **31** is an especially provocative structural feature that finds precedence in the crystallographic literature,[53] and a possible role in deaggregation has been mentioned.[54]

Autocatalysis. Catalysis by aryllithiums is also baffling. Previous studies of carbamate metalations[6a] offer a technically tractable system in which to study the condensation of an aryllithium with LDA dimer, revealing a rate-limiting transition structure of stoichiometry $[(i\text{-Pr}_2\text{NLi})_2(\text{ArLi})]^{\ddagger}$ (mixed trimers). It appeared that reactive LDA-lithiated carbamate mixed dimers interceded. Thus, we cannot say for certain whether the two instances of aryllithium-derived autocatalysis are completely analogous. Moreover, the studies described herein, showing that **2** is 6-fold more catalytically active than **3**, underscore the two critical prerequisites to observe autocatalysis: a reaction must be sensitive to catalysis, and a product (or byproduct) must be a viable catalyst. Evidence is accruing that failures to observe autocatalysis may trace to one or both requirements. Although details of *how* aryllithiums catalyze LDA deaggregation remain elusive, we are optimistic that mechanistic descriptions of salt-catalyzed LDA deaggregation will continue to evolve albeit obstinately.

Dimer- versus Monomer-Based Metalations in Review. Throughout this paper we have described uncatalyzed and catalyzed metalations as dimer- and monomer-based, respectively. One might be troubled, however, by the seemingly parallel behavior of the two classes showing an oddly similar THF-dependent regioselectivity. The monomer-based metalations are, to the maximum extent possible within our hands, unassailable. Are we sure, however, that the uncatalyzed metalations proceed via a different intermediate? There is no question that highly solvated tetramers (implicated triple ions) give us pause.

We attribute the uncatalyzed metalations to dimer-based mechanisms based on four lines of reasoning: (1) although not really evidence per se, the computational studies show that both dimer- and triple-ion-based metalations are highly competent; (2) the regioselectivities for LiCl- and ArLi-catalyzed reactions are indistinguishable, yet the regioselectivity for the uncatalyzed metalations is reversed and differs by an overall factor of >2; (3) competitive isotope effects for metalation to form both **2** and **3** are higher for uncatalyzed than LiCl-catalyzed metalation (although the differences are nearing our limits of distinction); (4) **1**-2,6-d_2 displays a nearly first-order LDA dependence under conditions of rate-limiting deuterium transfer. Point 4 seems to put to rest what had been a persistently circumstantial case for dimer-based metalation. We are unsure, however, how many structurally distinct aggregated forms can be intercepted by reactive substrates; this topic is being actively studied.

CONCLUSION

We conclude this paper in a somewhat unorthodox way by considering the consequences of the work from two very different perspectives. In the first, we address those interested in mechanistic organolithium chemistry. This viewpoint was most certainly the primary focus of the paper. In the second, we try to imagine what the ortholithiation of **1** might look like to a synthetic chemist peering through a largely empirical lens.

Mechanistic Organolithium Perspective. One could legitimately ask why LDA-mediated reactions in THF at −78 °C are proving so complex compared with their counterparts at elevated temperatures.[23] To answer this question, we offer the ensemble of aggregates en route to LDA monomer in Scheme 8. The structures are not just figments of our imaginations but rather computationally legitimate minima that will be described in the next paper of this series.[6] The computed barriers separating them are, with the exception of the first solvation step,[55] surprisingly high (>10 kcal/mol) relative to dimeric LDA in its resting state **4**, and the barriers are at notably comparable energies.

For substrates of relatively low reactivity the equilibria in Scheme 8 are rapid on the time scales of reactions with the substrate. All species are available to react, and 25 years of accumulated rate studies confirm that many do.[23] Now imagine monotonically increasing the reactivity of the substrate; instead of following the kinetics over shorter time scales, we simply reduce the reaction temperatures to monitor the reaction on convenient laboratory time scales. At some level of reactivity (at some temperature required to monitor reaction rates conveniently using standard analytical methods) the rates that substrates react with LDA aggregates become comparable to those at which the aggregates exchange. Through an odd twist of fate, this critical temperature for LDA/THF is at or near −78 °C.

Evidence is accruing that highly reactive substrates can intercept LDA at various stages of deaggregation, rendering aggregation events rate limiting and the conditions decidedly nonequilibrating. Simplistic thinking early on led us to surmise that a rate-limiting deaggregation would be substrate independent and that all substrates above some threshold of reactivity would react at precisely the same rate. We realized, however, that intercepting different fleeting intermediates would necessarily lead to substrate-dependent rates *even if the rates were independent of the substrate concentration*. Substrates also may participate in a critical deaggregation or complexation event but with the key reaction of interest (proton transfer, for example) occurring as a post-rate-limiting step. In this scenario, even substrate concentration dependencies could be affiliated with an aggregation-limiting transformation.

Of course, LiX-catalyzed deaggregation adds a further layer of complexity in the form of a hypersensitivity to LiCl contaminants and accelerations elicited by autocatalysis. The appearance of autocatalysis and its virulence depend on both the catalytic efficacy of the lithium salt being formed *and* on a mechanistic advantage of the catalyzed deaggregation. Enolates, for example, are particularly poor autocatalysts[6] compared with aryllithiums, aryllithiums display autocatalysis that depends on the substituents on the arene (as in **2** and **3**), and the catalytic activity of all salts studied to date pale in comparison with LiCl.[6]

dx.doi.org/10.1021/ja200906z |*J. Am. Chem. Soc.* 2011, 133, 7135–7151

Scheme 9

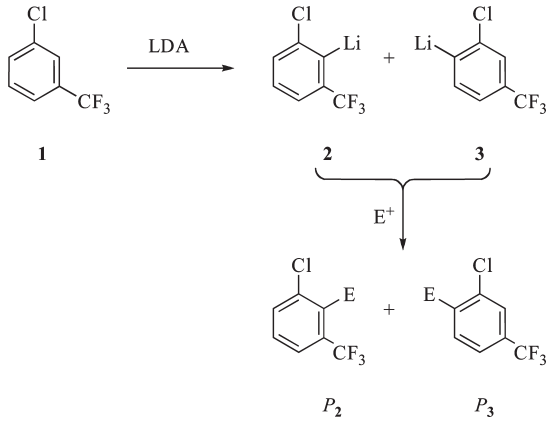

As we gather insights about LDA-mediated reactions under conditions in which aggregates are not at full equilibrium, we are constantly re-evaluating published conclusions.[56] Case studies considered in isolation can be fully self-consistent whereas results from different case studies can conflict. As a simple example, LiCl-catalyzed deaggregation is sensitive to the substrate, appearing as a first-order dependence on LiCl concentration in one case[3] and second-order dependencies in others.[6b−d] A fully self-consistent holistic view is beyond our gaze.

Synthetic Chemistry Perspective. Now consider the chemistry from the vantage point of a synthetic chemist who relies less on mechanism and more on empiricism and instinct. Schlosser and co-workers, for example, studied the metalation of **1**, but we can neither retrace their experience nor would we describe them as generic empiricists.[1] Let us assume the hypothetical synthetic chemist is you.

Imagine you metalate **1** and quench the intermediate aryllithiums to form regioisomeric products P_2 and P_3 (Scheme 9). You begin by generating LDA in situ from commercial *n*-BuLi and diisopropylamine and quenching the reaction with an efficient electrophile (maybe benzaldehyde).[57] What you could not possibly know is that the metalation is dramatically accelerated by the LiCl contaminant in the *n*-BuLi. What you *observe* is that the metalation is complete within only a minute or two, and a prompt quench affords regioisomers P_2 and P_3 in an uninspiring 2:1 ratio. As a consummate empiricist, you heed a previous assertion that THF *concentration* is a critical variable[23] and carry out the reaction using 2.0 M THF. Once again, what you would not know is that the regioselectivity under the auspices of LiCl catalysis derives from differentially solvated monomers. You would observe that using low THF concentration in a hydrocarbon cosolvent promotes the formation of regioisomer P_2 (up to 5:1 selectivity for **2**). You might also notice that the metalation is a little slower, requiring delayed quenching to obtain a good yield.

Beneath the surface of the kinetically controlled regioselectivities lurks a diisopropylamine-catalyzed equilibration of **2** and **3**. Such aryllithium equilibrations are well documented.[4,5] Varying the time allowed for the metalation by as little as 10 min is sufficient to alter the regioselectivity owing to this equilibration. Frustration caused by erratic selectivities is easy to imagine. You would likely discover, whether through intent or by chance, that the selectivity for **2** improves with protracted metalation at −78 °C or by warming (but below −20 °C to preclude benzyne formation).[58] Product P_2 derived from aryllithium **2** can be isolated in >40:1 selectivity. Diisopropylamine added at the outset would also accelerate the equilibration.

For the sake of discussion, let us assume that you require the more elusive product P_3. Of course, timely quenching with the electrophile is already established as essential to retain maximal (albeit disappointing) selectivity for P_3. You decide to try commercially available LDA as the THF solvate rather than prepare your LDA in situ. (It is certainly more convenient.) Alas, commercial LDA is often uncontaminated by catalytically active LiCl. (Halide-free commercial LDA lists ethyl benzene as a component.) Imagine your surprise when metalation and prompt quenching elevates the selectivity (the dimer-based metalations are, afterall, slightly more selective for **3**) but the isolated yield collapses to <10% owing to low conversion. If you are a pharmaceutical process chemist working on large scale, this result would be an unmitigated disaster. A graduate student might simply titrate the LDA, show that the reported titer is valid, and, once again, isolate a terrible yield of product. A third attempt with protracted stirring reveals that the metalation does occur but slowly. It is now obvious that commercial LDA offers little advantage because the slight bias toward formation of **3** is eroded by the equilibration of **3** to **2** during protracted reaction times. You could have enjoyed the convenience and greater safety[59] of commercial LDA with the activity of LDA prepared in situ by adding a few mole percent LiCl generated using Et_3NHCl.[18]

By this time, your quest to prepare P_3 via **3** would have led to other bases. Success is achieved: whereas *n*-BuLi gives a 4:1 selectivity favoring **2**, either *sec*-BuLi or LiTMP affords **3** in 20:1 selectivity.[1,60] Possibly not realizing that the hindrance of the tetramethylpiperidine byproduct completely suppresses amine-mediated equilibration, you invoke a model based on purely steric effects, declare victory, and move on to the next step.

EXPERIMENTAL SECTION

Reagents and Solvents. THF and hexane were distilled from blue or purple solutions containing sodium benzophenone ketyl. The hexane contained 1% tetraglyme to dissolve the ketyl. $Et_3N\cdot HCl$ was recrystallized from THF/2-propanol.[18] Literature procedures[61] were modified to prepare LDA as a LiCl- and ligand-free solid.[3] Solutions of LDA were titrated using a literature method.[62] Deuterated substrates were prepared as described below.

IR Spectroscopic Analyses. IR spectra were recorded using an in situ IR spectrometer fitted with a 30-bounce, silicon-tipped probe. The spectra were acquired in 16 scans at a gain of 1 and a resolution of 4 cm^{-1}. A representative reaction was carried out as follows: The IR probe was inserted through a nylon adapter and O-ring seal into an oven-dried, cylindrical flask fitted with a magnetic stir bar and a T-joint. The T-joint was capped by a septum for injections and a nitrogen line. After evacuating under full vacuum, heating, and flushing with nitrogen, the flask was charged with LDA (108 mg, 1.01 mmol) in THF and cooled in a dry ice−acetone bath prepared from fresh acetone. [Preparation of the same solution but containing 5.0 mol % LiCl (0.005 M) requires the addition of a LiCl stock solution (0.50 mL) prepared from $Et_3N\cdot HCl$ (27.5 mg, 0.20 mmol) and LDA (25.0 mg, 0.23 mmol) in 2.0 mL THF.] After recording a background spectrum, we added arene **1** (0.76 mmol) with stirring. For the most rapid reactions, IR spectra were recorded every 3 s over the course of the reaction, monitoring the absorbance at 1325 cm^{-1}.

NMR Spectroscopic Analyses. All NMR samples were prepared using stock solutions and sealed under partial vacuum. Standard ^6Li, ^{13}C, ^{15}N, and ^{19}F NMR spectra were recorded on a 500 MHz spectrometer at 73.57, 125.79, 50.66, and 470.35 MHz (respectively). The ^6Li, ^{13}C, and ^{15}N resonances are referenced to 0.30 M [^{6}Li]LiCl/MeOH at −90 °C

(0.0 ppm), the CH_2O resonance of THF at −90 °C (67.57 ppm), and neat Me_2NEt at −90 °C (25.7 ppm), respectively.

2-Deutero-1-chloro-3-(trifluoromethyl)benzene (1-2-*d*). Using a method published by Knochel,[14] commercially available 2-bromo-1-chloro-3-(trifluoromethyl)benzene (4.86 g, 18.7 mmol, 1.0 equiv) was added via syringe to a 1.3 M THF solution of isopropylmagnesium chloride−LiCl complex (29.0 mL, 22.3 mmol, 1.2 equiv) in dry THF at 0 °C under argon. After the solution was stirred for 20 min, 10 equiv of deuterium oxide (3.7 mL) was added to the solution. The mixture was allowed to warm to room temperature, and the pH was adjusted to 1.0 with 2.0 M aqueous HCl solution to dissolve all salts. Organic and aqueous layers were separated, and the aqueous layer was washed with 3 × 20 mL Et_2O. The organic layers were combined, dried over granular Na_2SO_4, and distilled, and **1**-2-*d* was collected at 135 °C as a colorless liquid (3.69 g, 14.2 mmol) in 76% yield. ^{1}H NMR δ 7.52 (m, 2H), 7.43 (m, 1H). ^{13}C NMR δ 135.2 (s), 132.6 (q, $^2J_{C-F}$ = 33 Hz), 132.1 (s), 130.2 (s), 125.5 (tq, $^2J_{C-D}$ = 26 Hz, $^2J_{C-F}$ = 4.0 Hz), 123.8 (q, $^2J_{C-F}$ = 272 Hz), 123.4 (q, $^2J_{C-F}$ = 4.0 Hz).

6-Deutero-1-chloro-3-(trifluoromethyl)benzene (1-6-*d*). The compound was synthesized as above from commercially available 6-bromo-1-chloro-3-(trifluoromethyl)benzene, and **1**-6-*d* was collected at 135 °C as a colorless liquid (3.9 g, 15.0 mmol) in 80% yield. ^{1}H NMR δ 7.62 (s, 1H), 7.52 (m, 1H), 7.43 (m, 1H). ^{13}C NMR δ 135.0 (s), 132.5 (q, $^2J_{C-F}$ = 33 Hz), 131.9 (t, $^2J_{C-D}$ = 26 Hz), 130.2 (s), 125.8 (q, $^2J_{C-F}$ = 4.0 Hz), 123.6 (q, $^2J_{C-F}$ = 4.0 Hz), 123.5 (q, $^2J_{C-F}$ = 272 Hz).

2,6-Dideutero-1-chloro-3-(trifluoromethyl)benzene (1-2,6-d_2). A 2.5 M solution of *n*-BuLi in hexane (14.8 mL, 37.0 mmol) was added via syringe pump to a solution of dry diisopropylamine (5.7 mL, 40.7 mmol) and $Et_3N\cdot$HCl (0.25 g, 1.85 mmol, 0.050 equiv) in 100 mL of dry THF at −78 °C under argon. After the solution was stirred for 20 min, **1** (5.0 mL, 37.0 mmol, 1 equiv) was added to the in situ generated LDA solution. After stirring at −78 °C for 30 min, *d*-MeOH (1.51 mL, 37.0 mmol, 1 equiv) was added. The process of sequential *n*-BuLi and *d*-MeOH addition of 1.0 equiv was repeated three more times. A final amount of *d*-MeOH (15 mL, 10 equiv) was added to fully quench the reaction. After the mixture was allowed to warm to room temperature, the pH was adjusted to 1.0 with 2.0 M HCl solution to dissolve all salts. Organic and aqueous layers were separated, and the aqueous layer was washed with 3 × 20 mL Et_2O. The organic layers were combined and dried over granular Na_2SO_4 and distilled, and **1**-2,6-d_2 was collected at 135 °C as a colorless liquid (3.74 g, 18.2 mmol) in 49% yield. ^{1}H NMR δ 7.52 (m, 1H), 7.43 (m, 1H). ^{13}C NMR δ 135.3 (s), 132.6 (q, $^2J_{C-F}$ = 33 Hz), 131.9 (t, $^2J_{C-D}$ = 26 Hz), 130.2 (s), 125.8 (tq, $^2J_{C-D}$ = 26 Hz, $^2J_{C-F}$ = 4.0 Hz), 123.8 (q, $^2J_{C-F}$ = 272 Hz), 123.5 (q, $^2J_{C-F}$ = 4.0 Hz).

Numeric Integrations. The time-dependent concentration plots obtained using IR spectroscopy are fit to a mechanistic model expressed by a set of differential equations. The curve-fitting operation minimizes chi-square in searching for the coefficient values (rate constants). The Levenberg−Marquardt algorithm[63] is used for the chi-square minimization and is a form of nonlinear, least-squares fitting. The fitting procedure implements numeric integration based on the backward differentiation formula[64] to solve the differential equations, yielding functions describing concentration versus time.

■ ASSOCIATED CONTENT

Supporting Information. NMR, rate, and computational data and a complete list of authors for ref 15. This material is available free of charge via the Internet at http://pubs.acs.org.

■ AUTHOR INFORMATION

Corresponding Author
dbc6@cornell.edu

■ ACKNOWLEDGMENT

We thank the National Institutes of Health (GM39764) and, in part, the National Science Foundation for direct support of this work.

■ REFERENCES

(1) Mongin, F.; Desponds, O.; Schlosser, M. *Tetrahedron Lett.* **1995**, *37*, 2767.

(2) (a) Quéguiner, G.; Marsais, F.; Snieckus; Epsztajn, J. *Adv. Heterocycl. Chem.* **1991**, *52*, 187. (b) Mongin, F.; Queguiner, G. *Tetrahedron* **2001**, *57*, 5897. (c) Mongin, F.; Queguiner, G. *Tetrahedron* **2001**, *57*, 4059. (d) Merino, P. *Prog. Heterocycl. Chem.* **1999**, *11*, 21.(e) Clayden, J. In *The Chemistry of Organolithium Compounds*; Rappoport, Z., Marek, I., Eds.; Wiley: New York, 2004; Vol. 1, p 495. (f) Caubere, P. In *Reviews of Heteroatom Chemistry*; MYU: Tokyo, 1991; Vol. 4, pp 78−139. (g) Caubere, P. *Chem. Rev.* **1993**, *93*, 2317. (h) Marsais, F.; Queguiner, G. *Tetrahedron* **1983**, *39*, 2009. (i) Collins, I. *Perkin 1* **2000**, 2845. (i) Schlosser, M.; Mongin, F. *Chem. Soc. Rev.* **2007**, *36*, 1161. (j) Hartung, C. G.; Snieckus, V. In *Modern Arene Chemistry*; Astruc, D., Ed.; Wiley-VCH: Weinheim, 2002; Chapter 10. (k) Snieckus, V. *Chem. Rev.* **1990**, *90*, 879. (l) Taylor, C. M.; Watson, A. J. *Curr. Org. Chem.* **2004**, *8*, 623.(m) Bakker, W. I. I.; Wong, P. L.; Snieckus, V. In *e-EROS*; Paquette, L. A., Ed.; John Wiley: New York, 2001.

(3) Ma, Y.; Hoepker, A. C.; Gupta, L.; Faggin, M. F.; Collum, D. B. *J. Am. Chem. Soc.* **2010**, *132*, 15610.

(4) (a) Cottet, F.; Schlosser, M. *Eur. J. Org. Chem.* **2004**, 3793. (b) Trecourt, F.; Mallet, M.; Marsais, F.; Quéguiner, G. *J. Org. Chem.* **1988**, *53*, 1367. (c) Comins, D. L.; LaMunyon, D. H. *Tetrahedron Lett.* **1988**, *29*, 773. (d) Eaton, P. E.; Cunkle, G. T.; Marchioro, G.; Martin, R. M. *J. Am. Chem. Soc.* **1987**, *109*, 948. (e) Bridges., A. J.; Patt, W. C.; Stickney, T. M. *J. Org. Chem.* **1990**, *55*, 773. (f) Trécourt, F.; Marsais, F.; Güngör, T.; Quéguiner, G. *J. Chem. Soc., Perkin Trans. 1* **1990**, 2409. (g) Gros, P. C.; Fort, Y. *Eur. J. Org. Chem.* **2009**, 4199. (h) Cottet, F.; Marull, M.; Lefebvre, O.; Schlosser, M. *Eur. J. Org. Chem.* **2003**, 1559. (i) Güngör, T.; Marsais, F.; Quéguiner, G. *J. Organomet. Chem.* **1981**, *215*, 139. (j) Fukuda, T.; Ohta, T.; Sudo, E.; Iwao, M. *Org. Lett.* **2010**, *12*, 2734.

(5) Viciu, M.; Gupta, L.; Collum, D. B. *J. Am. Chem. Soc.* **2010**, *132*, 6361.

(6) (a) Singh, K. J.; Hoepker, A. C.; Collum, D. B. *J. Am. Chem. Soc.* **2008**, *130*, 18008. (b) Gupta, L.; Hoepker, A. C.; Singh, K. J.; Collum, D. B. *J. Org. Chem.* **2009**, *74*, 2231. (c) Gupta, L. Ph.D. Thesis, Cornell University, Ithaca, NY, August 2010. (d) Hoepker, A. C. Ph.D. Thesis, Cornell University, Ithaca, NY, August 2011.

(7) For examples of reactions that are fast relative to the rates of aggregate−aggregate exchanges see: (a) McGarrity, J. F.; Ogle, C. A. *J. Am. Chem. Soc.* **1985**, *107*, 1810. (b) Jones, A. C.; Sanders, A. W.; Bevan, M. J.; Reich, H. J. *J. Am. Chem. Soc.* **2007**, *129*, 3492. (c) Thompson, A.; Corley, E. G.; Huntington, M. F.; Grabowski, E. J. J.; Remenar, J. F.; Collum, D. B. *J. Am. Chem. Soc.* **1998**, *120*, 2028. (d) Jones, A. C.; Sanders, A. W.; Sikorski, W. H.; Jansen, K. L.; Reich, H. J. *J. Am. Chem. Soc.* **2008**, *130*, 6060.

(8) A survey of approximately 500 total syntheses compiled by H. J. Reich and coworkers revealed LDA to be the most commonly used reagent. The database currently resides at http://www.chem.wisc.edu/areas/reich/syntheses/syntheses.htm.

(9) (a) Seebach, D. In *Proceedings of the Robert A. Welch Foundation Conferences on Chemistry and Biochemistry*; Wiley: New York, 1984; p 93. (b) Seebach, D. *Angew. Chem., Int. Ed. Engl.* **1988**, *27*, 1624. (c) Tchoubar, B.; Loupy, A. *Salt Effects in Organic and Organometallic Chemistry*; VCH: New York, 1992; Chapters 4, 5, and 7. (d) Caubère, P. *Chem. Rev.* **1993**, *93*, 2317.

(10) (a) Collum, D. B. *Acc. Chem. Res.* **1993**, *26*, 227. (b) Lucht, B. L.; Collum, D. B. *Acc. Chem. Res.* **1999**, *32*, 1035.

(11) (a) Kim, Y.-J.; Bernstein, M. P.; Galiano-Roth, A. S.; Romesberg, F. E.; Fuller, D. J.; Harrison, A. T.; Collum, D. B.; Williard, P. G.

J. Org. Chem. **1991**, *56*, 4435. (b) Collum, D. B. *Acc. Chem. Res.* **1993**, *26*, 227.

(12) ^{6}Li is spin 1. For a review of ^{6}Li NMR spectroscopy, see: Günther, H. *J. Braz. Chem. Soc.* **1999**, *10*, 241.

(13) (a) Espinet, P.; Albeniz, A. C.; Casares, J. A.; Martinez-Ilarduya, J. M. *Coord. Chem. Rev.* **2008**, *252*, 2180. (b) Gakh, Y. G.; Gakh, A. A.; Gronenborn, A. M. *Magn. Reson. Chem.* **2000**, *38*, 551. (c) McGill, C. A.; Nordon, A.; Littlejohn, D. *J. Process Anal. Chem.* **2001**, *6*, 36. (d) Espinet, P.; Albeniz, A. C.; Casares, J. A.; Martinez-Ilarduya, J. M. *Coord. Chem. Rev.* **2008**, *252*, 2180.

(14) Krasovskiy, A.; Knochel, P. *Angew. Chem., Int. Ed.* **2004**, *43*, 3333.

(15) Frisch, M. J.; et al. *Gaussian 03, revision B.04*; Gaussian, Inc.: Wallingford, CT, 2004.

(16) (a) Ramirez, A.; Candler, J.; Bashore, C. G.; Wirtz, M. C.; Coe, J. W.; Collum, D. B. *J. Am. Chem. Soc.* **2004**, *126*, 14700. (b) Riggs, J. C.; Ramirez, A.; Cremeens, M. E.; Bashore, C. G.; Candler, J.; Wirtz, M. C.; Coe, J. W.; Collum, D. B. *J. Am. Chem. Soc.* **2008**, *130*, 3406. (c) Kottke, T.; Sung, K.; Lagow, R. J. *Angew. Chem., Int. Ed. Engl.* **1995**, *34*, 1517. (d) Reich, H. J.; Green, D. P.; Medina, M. A.; Goldenberg, W. S.; Gudmundsson, B. Ö.; Dykstra, R. R.; Phillips, N. H. *J. Am. Chem. Soc.* **1998**, *120*, 7201. (e) Bonasia, P. J.; Arnold, J. *J. Organomet. Chem.* **1993**, *449*, 147.(f) Reference 6a.

(17) Galiano-Roth, A. S.; Kim, Y.-J.; Gilchrist, J. H.; Harrison, A. T.; Fuller, D. J.; Collum, D. B. *J. Am. Chem. Soc.* **1991**, *113*, 5053.

(18) Snaith and co-workers underscored the merits of R_3NHX salts as precursors to anhydrous LiX salts. See: Barr, D.; Snaith, R.; Wright, D. S.; Mulvey, R. E.; Wade, K. *J. Am. Chem. Soc.* **1987**, *109*, 7891. Also see: Hall, P. L.; Gilchrist, J. H.; Collum, D. B. *J. Am. Chem. Soc.* **1991**, *113*, 9571.

(19) Zhao, P.; Collum, D. B. *J. Am. Chem. Soc.* **2003**, *125*, 14411 and references cited therein.

(20) Rein, A. J.; Donahue, S. M.; Pavlosky, M. A. *Curr. Opin. Drug Discovery Dev.* **2000**, *3*, 734.

(21) (a) Espenson, J. H. *Chemical Kinetics and Reaction Mechanisms*, 2nd ed.; McGraw-Hill: New York, 1995; Chapter 2, p 44. (b) Atkins, P. W.; Jones, L. L. *Chemical Principles: The Quest for Insight*, 2nd ed.; W H. Freeman: New York, 2002. (c) Rae, M.; Berberan-Santos, M. N. *J. Chem. Educ.* **2004**, *81*, 436.

(22) Determining initial rates (slopes) of a curved decay can be strongly dependent on the percent conversion, requiring a compromise between adequate sample size and loss of linearity. This problem is mitigated by fitting a significant part of the decay, a portion that includes some curvature, to a third-order polynomial ($at^2 + bt + c$), making sure not to include too much curvature. The parameter b represents the rate at time zero. (One may verify this by taking the first derivative with respect to t and setting $t = 0$. Initial rate = $f'(0) = b$.) The experimental observable (NMR intensity, IR absorbance, etc.) is converted to concentration to ensure a valid comparison between initial rates of varying concentrations.

(23) For a review of rate studies of LDA-mediated reactions see: Collum, D. B.; McNeil, A. J.; Ramirez, A. *Angew. Chem., Int. Ed.* **2007**, *46*, 3002.

(24) The concentration of LDA, although expressed in units of molarity, refers to the concentration of the monomer unit (normality). The concentration of THF is expressed as total concentration of free (uncoordinated) ligand.

(25) The minor deviation above first order has the appearance of experimental error. A forthcoming study, however, describes experimental evidence of LDA-tetramer-based reactivities.

(26) We define the idealized rate law as that obtained by rounding the observed reaction orders to the nearest rational order.

(27) Open dimers were first proposed for the isomerization of oxiranes to allylic alcohols by mixed metal bases. See: Mordini, A.; Rayana, E. B.; Margot, C.; Schlosser, M. *Tetrahedron* **1990**, *46*, 2401. For a bibliography of lithium amide open dimers, see: Ramirez, A.; Sun, X.; Collum, D. B. *J. Am. Chem. Soc.* **2006**, *128*, 10326 and references cited therein.

(28) Competitive and intramolecular isotope effects can be used to examine post-rate-limiting proton transfer. They differ in that the intramolecular isotope effect demands a symmetry-equivalent choice of H versus D within the same molecule whereas the competitive isotope effect requires an exchange mechanism to establish the choice of H versus D.

(29) (a) Carpenter, B. K. *Determination of Organic Reaction Mechanisms*; Wiley: New York, 1984. (b) Whisler, M. C.; MacNeil, S.; Snieckus, V.; Beak, P. *Angew. Chem., Int. Ed.* **2004**, *43*, 2206.

(30) The calculated isotope effects in eqs 6 and 7 derive from the regioselectivities derived from **1**-2-d_1, and **1**-6-d_1. If the isotope effects are calculated using **1**-2,6-d_2 instead of **1**, the isotope effects are calculated as follows:

$$k_{H(2)}/k_{D(2)} = (k_{H(2)}/k_{D(6)})(k_{D(6)}/k_{D(2)}) = 50$$

$$k_{H(6)}/k_{D(6)} = (k_{H(6)}/k_{D(2)})(k_{D(2)}/k_{D(6)}) = 12$$

(31) The method used to prepare **1**-2,6-d_2, which involves initial metalation by LDA and quenching with MeOD (1.0 equiv) followed by alternating pulses of *n*-BuLi *without intermediate workups,* may have a general utility for exhaustive deuteration of the acidic sites on arenes.

(32) (a) Stegelmann, C.; Andreasen, A.; Campbell, C. T. *J. Am. Chem. Soc.* **2009**, *131*, 8077. (b) Maniscalco, S. J.; Tally, J. F.; Fisher, H. F. *Arch. Biochem. Biophys.* **2004**, *425*, 165.

(33) (a) Isotopic perturbation is insufficient to resolve the resonances of **1** and **1**-2,6-d_2 by ^{19}F NMR spectroscopy.[33b−d] The IR absorbances of **1** (1428 cm^{-1}) and **1**-2,6-d_2 (1384 cm^{-1}) could be monitored, but with some error introduced by absorbances of the aryllithiums. (b) Hindermann, D. K.; Cornwell, C. D. *J. Chem. Phys.* **1968**, *48*, 4148. (c) Forsyth, D. A.; Yang, J.-R. *J. Am. Chem. Soc.* **1986**, *108*, 2157. (d) Lambert, J. B.; Greifenstein, L. G. *J. Am. Chem. Soc.* **1973**, *95*, 6150.

(34) For an attempted comprehensive bibliography of anionic triple ions of lithium salts (X−Li−X$^-$), see: Ma, Y.; Ramirez, A.; Singh, K. J.; Keresztes, I.; Collum, D. B. *J. Am. Chem. Soc.* **2006**, *128*, 15399.

(35) The computations use the Gaussian standard state of 1.0 atm. If the THF concentration is corrected to neat THF (approximately 12 M), each solvation step benefits from approximately 2.0 kcal/mol of additional stabilization at −78 °C (195 K). Pratt, L. M.; Merry, S.; Nguyen, S. C.; Quan, P.; Thanh, B. T. *Tetrahedron* **2006**, *62*, 10821.

(36) Frey, P. A.; Hegeman, A. D. *Enzymatic Reaction Mechanisms*; Oxford University Press: New York, 2007; Chapter 2.

(37) LDA-mediated ortholithiations of 2-fluoropyridines also show a second-order catalysis by LiCl.[6c]

(38) (a) Ma, Y.; Collum, D. B. *J. Am. Chem. Soc.* **2007**, *129*, 14818. (b) Depue, J. S.; Collum, D. B. *J. Am. Chem. Soc.* **1988**, *110*, 5524. (c) Galiano-Roth, A. S.; Collum, D. B. *J. Am. Chem. Soc.* **1989**, *111*, 6772.

(39) Laurence, C.; Nicolet, P.; Dalati, M. T.; Abboud, J.-L. M.; Notario, R. *J. Phys. Chem.* **1994**, *98*, 5807.

(40) (a) Lucht, B. L.; Collum, D. B. *J. Am. Chem. Soc.* **1994**, *116*, 6009. (b) Remenar, J. F.; Lucht, B. L.; Collum, D. B. *J. Am. Chem. Soc.* **1997**, *119*, 5567.

(41) Equation 17 appears to become undefined at $[LiCl_T] = 0$, but this is not the case as described previously.[3]

(42) (a) Besson, C.; Finney, E. E.; Finke, R. G. *J. Am. Chem. Soc.* **2005**, *127*, 8179. (b) Besson, C.; Finney, E. E.; Finke, R. G. *Chem. Mater.* **2005**, *17*, 4925. (c) Huang, K. T.; Keszler, A.; Patel, N.; Patel, R. P.; Gladwin, M. T.; Kim-Shapiro, D. B.; Hogg, N. *J. Biol. Chem.* **2005**, *280*, 31126. (d) Huang, Z.; Shiva, S.; Kim-Shapiro, D. B.; Patel, R. P.; Ringwood, L. A.; Irby, C. E.; Huang, K. T.; Ho, C.; Hogg, N.; Schechter, A. N.; Gladwin, M. T. *J. Clin. Invest.* **2005**, *115*, 2099. (e) Tanj, S.; Ohno, A.; Sato, I.; Soai, K *Org. Lett.* **2001**, *3*, 287. (f) Barrios-Landeros, F.; Carrow, B. P.; Hartwig, J. F. *J. Am. Chem. Soc.* **2008**, *130*, 5842.

(43) (a) Depue, J. S.; Collum, D. B. *J. Am. Chem. Soc.* **1988**, *110*, 5524. (b) McNeil, A. J.; Toombes, G. E. S.; Gruner, S. M.; Lobkovsky, E.; Collum, D. B.; Chandramouli, S. V.; Vanasse, B. J.;

Ayers, T. A. *J. Am. Chem. Soc.* **2004**, *126*, 16559. (c) Nudelman, N. S.; Velurtas, S.; Grela, M. A. *J. Phys. Org. Chem.* **2003**, *16*, 669. (d) Alberts, A. H.; Wynberg, H. *J. Am. Chem. Soc.* **1989**, *111*, 7265. (e) Alberts, A. H.; Wynberg, H. *J. Chem. Soc., Chem. Commun.* **1990**, 453.

(44) The principle of microscopic reversibility seems to have been the source of frequent controversies and must be applied with caution. It is not obvious to us, for example, that the following authors, all warning of the risks, would agree with each other's assertions: (a) Blackmond, D. G. *Angew. Chem., Int. Ed.* **2009**, *48*, 2648. (b) Krupka, R. M.; Kaplan, H.; Laidler, K. J. *J. Chem. Soc., Faraday Trans.* **1966**, *62*, 2754. (c) Chandrasekhar, S. *Res. Chem. Intermed.* **1992**, *17*, 173. (d) Burwell, R. L.; Pearson, R. G. *J. Phys. Chem.* **1966**, *70*, 300.

(45) For a discussion of the mechanistic basis of cooperative substituent effects in ortholithiation, see: Chadwick, S. T.; Ramirez, A.; Gupta, L.; Collum, D. B. *J. Am. Chem. Soc.* **2007**, *129*, 2259.

(46) (a) Chadwick, S. T.; Rennels, R. A.; Rutherford, J. L.; Collum, D. B. *J. Am. Chem. Soc.* **2000**, *122*, 8640. (b) Anderson, D. R.; Faibish, N. C.; Beak, P. *J. Am. Chem. Soc.* **1999**, *121*, 7553. (c) Singh, K. J.; Collum, D. B. *J. Am. Chem. Soc.* **2006**, *128*, 13753. (d) Meyers, A. I.; Mihelich, E. D. *J. Org. Chem.* **1975**, *40*, 3158. (e) Ramirez, A.; Sun, X.; Collum, D. B. *J. Am. Chem. Soc.* **2006**, *128*, 10326. (f) Sun, X.; Collum, D. B. *J. Am. Chem. Soc.* **2000**, *122*, 2452. (g) Ma, Y.; Breslin, S.; Keresztes, I.; Lobkovsky, E.; Collum, D. B. *J. Org. Chem.* **2008**, *73*, 9610.

(47) (a) Ruszczycky, M. W.; Anderson, V. E. *J. Theor. Biol.* **2006**, *243*, 328. (b) Ray, W. J., Jr. *Biochemistry* **1983**, *22*, 4625.

(48) (a) Gregory, K.; Schleyer, P. v. R.; Snaith, R. *Adv. Inorg. Chem.* **1991**, *37*, 47. (b) Mulvey, R. E. *Chem. Soc. Rev.* **1991**, *20*, 167. (c) Beswick, M. A.; Wright, D. S. In *Comprehensive Organometallic Chemistry II*; Abels, E. W., Stone, F. G. A., Wilkinson, G., Eds.; Pergamon Press: New York, 1995; Vol. 1, Chapter 1. (d) Mulvey, R. E. *Chem. Soc. Rev.* **1998**, *27*, 339. (e) Rutherford, J. L.; Collum, D. B. *J. Am. Chem. Soc.* **1999**, *121*, 10198.

(49) A four-rung LDA/LiX ladder has been characterized: Williard, P. G.; Hintze, M. J. *J. Am. Chem. Soc.* **1987**, *109*, 5539.

(50) Romesberg, F. E.; Collum, D. B. *J. Am. Chem. Soc.* **1994**, *116*, 9198.

(51) (a) Evans, W. J.; Broomhall-Dillard, R. N. R.; Ziller, J. W. *J. Organomet. Chem.* **1998**, *569*, 89. (b) Klingebiel, U.; Tecklenburg, B.; Noltemeyer, M.; Schmidt-Baese, D.; Herbst-Irmer, R. *Z. Naturforsch., B: J. Chem. Sci.* **1998**, *53*, 355.

(52) The most stable lithium cation $[+Li(THF)_5]$ and most stable triple ion $\{[(THF)_4LiClLi(THF)_3]^+\}$ are related as follows:

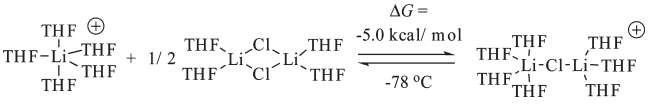

For related computations, see: Yakimansky, A. V.; Müller, A. H. E.; Van Beylen, M. *Macromolecules* **2000**, *33*, 5686.

(53) Representative examples of structurally characterized bridging THF ligands: (a) Pratt, L. M.; Merry, A.; Nguyen, S. C.; Quanb, P.; Thanh, B. T. *Tetrahedron* **2006**, *62*, 10821. (b) Clegg, W.; Liddle, S. T.; Mulvey, R. E.; Robertson, A. *Chem. Commun.* **1999**, 511. (c) Boche, G.; Boie, C.; Bosold, F.; Harms, K.; Marsch, M. *Angew. Chem., Int. Ed.* **1994**, *33*, 115. (d) Daniele, S.; Drost, C.; Gehrhus, B.; Hawkins, S. M.; Hitchcock, P. B.; Lappert, M. F.; Merle, P. G.; Bott, S. G. *J. Chem. Soc., Dalton Trans.* **2001**, 3179. (e) Chivers, T.; Fedorchuk, C.; Parvez, M. *Inorg. Chem.* **2004**, *43*, 2643. (f) Briand, G. G.; Chivers, T.; Parvez, M. *J. Chem. Soc., Dalton Trans.* **2002**, 3785.

(54) Clegg, W.; Horsburgh, L.; Mackenzie, F. M.; Mulvey, R. E. *J. Chem. Soc., Chem. Commun.* **1995**, 2011.

(55) THF exchange on LDA is too fast to monitor by NMR spectroscopy, but it is calculated to occur with activation barriers of <4 kcal/mol.[6d]

(56) During the following carbamate metalation[6a]

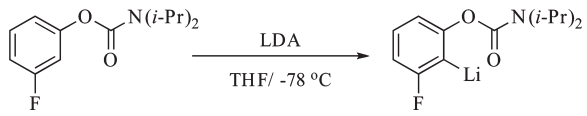

two concerns lingered: the metalation displayed an unexpectedly small isotope effect (k_H/k_D = 3−4), and a plot of rate versus concentration showed a first-order arene dependence but with a downward curvature that looks suspiciously like an incomplete version of the saturation curve in Figure 7. Indeed, we have now found a large competitive isotope effect (k_H/k_D > 30), suggesting that the first-order dependence does *not* involve proton transfer and that deuterium transfer is partially rate limiting.

(57) Trapping experiments can be unreliable measures of the rates because they generate catalytically active lithium salts. Trimethylchlorosilane, for example, generates LiCl, rendering LiCl-sensitive arene lithiations nearly instantaneous. We chose benzaldehyde for our hypothetical example because alkoxides are not active deaggregation catalysts.[6]

(58) Warming to −20 °C in the presence of spiro[2.4]hepta-4,6-diene shows no evidence of trapping products. We do, however, see evidence of *n*-BuLi adducts if metalations with *n*-BuLi are allowed to inadvertently warm. Leading reference to benzyne formation: Riggs, J. C.; Ramirez, A.; Cremeens, M. E.; Bashore, C. G.; Candler, J.; Wirtz, M. C.; Coe, J. W.; Collum, D. B. *J. Am. Chem. Soc.* **2008**, *130*, 3406.

(59) Kopach, M. E.; Kobierski, M. E.; Coffey, D. S.; Alt, C. A.; Zhang, T.; Borghese, A.; Trankle, W. G.; Roberts, D. J. *Org. Process Res. Dev.* **2010**, *14*, 1229.

(60) The observed selectivities for the metalation of **1** by *n*-BuLi and *sec*-BuLi show approximately 3-fold higher proportions of **2** relative to **3** as the arene concentration goes from 0.05 equiv of **1** to 1.0 equiv of **1**. This result appears to be a kinetic consequence of mixed aggregates favoring formation of **3**. For references to structures and reactivities of *n*-BuLi/RLi ensembles, see: Chase, P. A.; Lutz, M.; Spek, A. L.; Gossage, R. A.; van Koten, G. *Dalton Trans.* **2008**, 5783.

(61) (a) Marck, W.; Huisgen, R. *Chem. Ber.* **1960**, *93*, 608. (b) Gaudemar-Bardone, F.; Gaudemar, M. *Synthesis* **1979**, 463. (c) Reetz, M. T.; Maier, W. F. *Liebigs Ann. Chem.* **1980**, 1471. (d) Williard, P. G.; Carpenter, G. B. *J. Am. Chem. Soc.* **1986**, *108*, 462. Williard, P. G.; Salvino, J. M. *J. Org. Chem.* **1993**, *58*, 1.(e) Morrison, R. C.; Hall, R. W.; Rathman, T. L. U.S. Patent 595,779, June 17, 1986.

(62) Kofron, W. G.; Baclawski, L. M. *J. Org. Chem.* **1976**, *41*, 1879.

(63) For an explanation of Levenberg−Marquardt nonlinear least-squares optimization, see: Press, W. H.; Flannery, B. P.; Teukolsky, S. A.; Vetterling, V. T. *Numerical Recipes in C*; Cambridge University Press: London, 1988; Chapter 14.4.

(64) Brown, P. N.; Byrne, G. D.; Hindmarsh, A. C. *J. Sci. Stat. Comput.* **1989**, *10*, 1038.